Adaptive Baseband Interference Cancellation for Full Duplex Wireless Communication Systems

by

Sanjay Avasarala

A Thesis Presented in Partial Fulfillment
of the Requirements for the Degree
Master of Science

Approved April 2016 by the
Graduate Supervisory Committee:

Sayfe Kiaei, Chair
Bertan Bakkaloglu
Jennifer Kitchen

ARIZONA STATE UNIVERSITY

May 2016

ABSTRACT

Traditional wireless communication systems operate in duplexed modes i.e. using time division duplexing or frequency division duplexing. These methods can respectively emulate full duplex mode operation or realize full duplex mode operation with decreased spectral efficiency. This thesis presents a novel method of achieving full duplex operation by actively cancelling out the transmitted signal in pseudo-real time. With appropriate hardware, the algorithms and techniques used in this work can be implemented in real time without any knowledge of the channel or any training sequence. Convergence times of down to 1 ms can be achieved which is adequate for the coherence bandwidths associated with an indoor environment. By utilizing adaptive cancellation, additional overhead for re-calibrating the system in other open-loop methods is not needed.

DEDICATION

Dedicated to my Parents and Friends.

ACKNOWLEDGMENTS

I would like to thank my advisor Dr. Kiaei for all the help and motivation he has provided me over the past years and throughout the duration of this project. Without his guidance I would not have come this far.

Moreover, I wish to thank our post-doc advisor Debashis Mandal for helping me with my project and guiding me through the entire design and experimentation process. I would also like to thank him for helping me with my final presentation and ensuring that everything would run smoothly. I am also grateful that I had the chance to sit with my colleagues who are all such wonderful folks.

I also extend my gratitude to my parents who have always taught me to work hard and were always there for me.

And finally I would like to thank my friends that I have made here in Tempe for allowing me to experience one of the most exciting times in my life.

TABLE OF CONTENTS

Page

CHAPTER Page

LIST OF TABLES

LIST OF FIGURES

CHAPTER 1

INTRODUCTION

Section 1.1. - Background

Traditional wireless communication systems contain both a radio frequency (RF) transmitter (TX) and receiver (RX). This type of system is known as a transceiver. There exist several traditional methods to successfully transmit and receive data at a maximum efficiency. These methods exploit three different areas: time, frequency, and space.

Time domain methods utilize what is known as Time Division Duplexing (TDD). TDD architectures will sequentially transmit and receive a signal i.e. the TX and RX will never simultaneously be powered on. Although this method uses a single frequency, the major drawback lies in the fact that twice the time is needed to successfully transmit and receive a data packet of equal size.

Frequency domain methods employ Frequency Division Duplexing (FDD). In this architecture, the TX and RX will be operating simultaneously but at different frequencies. Both chains will have Band Pass Filters (BPF) tuned to their specific frequency to block out any residual interference that may fall in each respective band. The obvious setback of this architecture is that twice the maximally efficient bandwidth is needed. With the rising number of users and cost of bandwidth, FDD technology may not be adequate.

A system that employs spatial methods will use directional antennas, antenna diversity, or cross-polarization techniques. Multiple Input Multiple Output (MIMO) systems use multiple antennas to increase throughput by delegating more packets of data to each antenna. Theoretically this accommodates for the loss in spectral efficiency or time

by effectively doubling throughput; however, additional real estate for multiple antennas is needed.

Section 1.2. – Motivation and explanation

Regarding the need for more spectrally efficient systems, it is clear that full duplex architectures are a solution. Full duplex systems can exist using two methods – active or passive echo cancellation. Figure 1.1 shows what kind of signals will be received from a transmitter operating at full power (significant harmonic distortion). In this case, a Double Side Band Suppressed Carrier (DSB-SC) type sin wave will be used to show distortion from 2nd and 3rd order effects. It also must be noted that this particular architecture uses two antennas placed at a set distance.

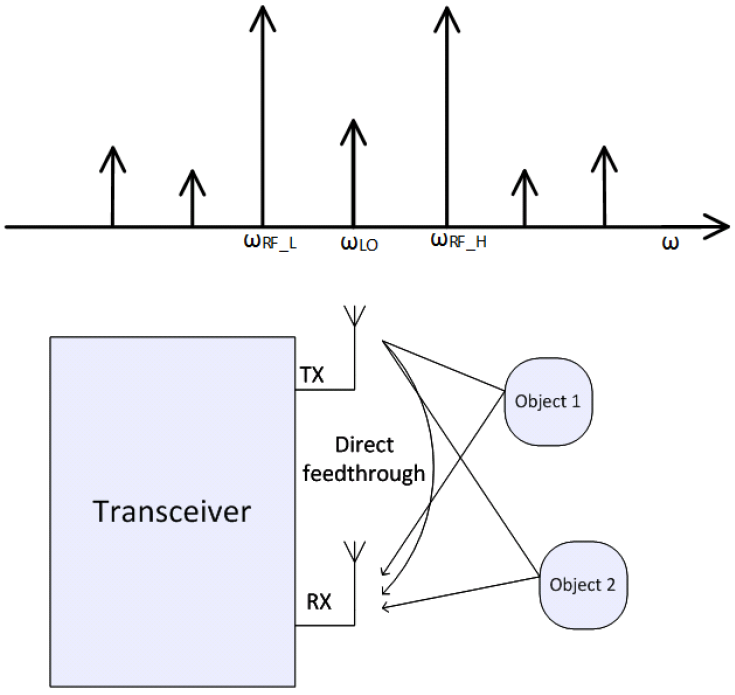

Figure 1.1 The transmitted signal is distorted and corrupted by multipath and non-linearity before it reaches the receiver.

Passive cancellation techniques typically rely on attenuating the transmitted signal before it reaches the receiver. Directional antennas or circulators can serve this purpose. According to [1] both active and passive cancellation techniques should be used to maximize transmit signal cancellation and achieve full duplex communication.

There exist three areas in a transceiver in which cancellation can be performed. These areas are at RF, analog baseband, and in the digital domain after quantization. It is preferred that cancellation is performed before the ADC otherwise the self-interference signal will saturate the dynamic range of the ADC and prevent the actual signal from being scaled up to the full scale range. However, there exists a trade-off in this scenario. The cancellation performed in the digital realm will be less effective if the received self-interference signal is weaker at the input of the ADC [6]. The total cancellation (analog and digital combined) will ultimately end up being equal despite the amount of cancellation that happens in either the digital or baseband analog realm.

Section 1.3. – Previous Work

Many papers have been published regarding the theory and implementation of full duplex systems. Researchers at Stanford have shown that WiFi 802.11ac systems at 2.45 GHz can successfully operate using full duplex methods [1]. They employed both analog RF and digital cancellation methods to maximize the suppression of the self-interference signal using the Wireless Open Access Research Platform (WARP) platform. In addition, a single antenna with a circulator was used to preserve real estate and provide additional cancellation. The analog RF cancellation was implemented using fixed delay lines with

variable attenuators per line that were tapped from the transmit path. This essentially emulates a Finite Impulse Response (FIR) filter in the analog domain. This allows the cancellation path to account for multi-path effects and also takes into account the noise and harmonics created by the transmitter itself. By using delayed versions of the signal from before and after the main self-interference delay, the received signal can be recreated in a fashion similar to sinc interpolation. Likewise, their digital algorithm tries to predict the current value by using previous and future samples known to the system.

The biggest issue with [1] is the fact that the cancellation algorithms are not online. This means that a certain time (900-1000 μs) will elapse before the circuits and digital algorithms adapt to the new environment. This might not pose a problem in a slow fading channel; however, in a fast fading channel with a short coherence time, the cancellation coefficients may not update fast enough. Moreover, WiFi preamble information about the channel is required to initialize the coefficients. Finally, the method they use to set the analog cancellation coefficients involves physically measuring the transfer function of each delay line. Despite the fact that this measurement only needs to be done once, mass-producing devices with this implementation will be problematic.

Stanford has also investigated a method of cancellation known as antenna cancellation [2]. Two TX antennas are placed on either side of the RX antenna such that there exists a spacing of $d + \frac{\lambda}{2}$ between one TX and RX pair and d between the other pair. This will result in an offset spacing of one half wavelength between the two TX antennas which causes destructive interference directly at the position of the RX antenna. The limitations of this design include bandwidth, power, and the channel center frequency. This implementation will not be useful at lower frequencies due to the large wavelengths

involved. In addition, the powers of the two TX antennas are required to be the same to achieve maximum nulling at the point of interest. The two TX antennas will also cause nulls at other points in the environment that results in dead spots. Moreover, the antenna placement needs to be manually implemented which may not be practical for an adaptive system in the field. Work in [5] explains that Orthogonal Frequency Division Multiplex (OFDM) systems will suffer from this architecture since each sub-carrier will experience a significant change in self-interference. Since the architecture needs three antennas, employing MIMO techniques may as well be used since a 3x3 system can theoretically triple throughput. The advantage of this architecture, however, is that no knowledge of the channel is needed and no calibration or coefficients need to be updated. Noise and harmonics from the transmitter are also cancelled out.

Researchers from Rice University successfully implemented a full duplex system using two separate antennas placed at a set distance in addition to analog RF and digital cancellation [3]. They also used the WARP platform to perform cancellation measurements. Although they were able to show good cancellation results, the bandwidth used was only 625 kHz. Moreover, the antenna spacing amounts they used were 20 cm and 40 cm; this will not be feasible for any sort of mobile device. The methods by which they implemented their algorithms and analog cancellation circuitry are not known.

Further research from Rice University investigated the effects of directional antennas in a base station [4]. Specifically, the half-power beamwidth angle of the antennas was varied to observe how cancellation degrades. The results of this study showed that directionality definitely improves the cancellation of the self-interference signal. The issue with directionality is that the range of transmission is now limited to the beamwidth angle

and the base station design is constrained by the placement of the antennas to achieve an angle that allows for maximum cancellation.

An architecture suggested in [5] uses a balun to invert the TX signal before injecting it into the RX chain before the mixer. Due to the relatively wide bandwidth of a balun, self-interference cancellation can work up to 100 MHz. The delay between the TX and RX path is corrected using a gradient descent algorithm that controls a delay element between the balun and the injection point. However, this method fails to address multi-path effects. The digital cancellation method used in [5] relies on the OFDM training symbols. They are initially defined in the frequency domain so an Inverse Fast Fourier Transform (IFFT) needs to be performed on the training symbols to recover the impulse response of the channel. The transmitted data is then convolved with this impulse response to create a predicted self-interference signal. Since the channel is a causal LTI system, the channel can be emulated using an FIR filter. The FIR filter coefficients can only be updated per every training pilot sent in an OFDM implying that this system is not truly 'online'. In addition, [5] states that there must be an absence of interference during the training sequence. This will be an issue in an environment rich with EM signals at that particular band, however, all active echo cancellation schemes will suffer from this effect. As stated earlier, coherence time will affect that rate that is needed to update the coefficients of the FIR filter [1]. Work in [5] claims that a static environment will have a coherence time on the order of seconds and thus an estimation update rate of a few hundred milliseconds will be sufficient.

Digital cancellation and its implementation is investigated in [7]. The architecture is similar to that of [1], however, only a causal FIR filter is used. An algorithm estimates

the number of taps needed based on the rms delay spread of the channel. The coefficients of the FIR filter are updated based on pilot tones and thus there exists overhead in this scheme and the implementation is not true real-time.

An experiment was performed on the impact of phase noise on active cancellation [6]. A test setup was created to mimic active echo cancellation. A known signal was first upconverted to RF and then fed to a splitter. The two splitter outputs were then fed to a vector signal analyzer (VSA) which downcoverted the signals using knowledge of the carrier frequency. The baseband signals were digitized with a sample rate of about 48 Msps. To emulate the active cancellation, the two signals were subtracted from each other after scaling and delaying. It was found that, theoretically, if the signals are only corrupted by delay and noise, cancellation is independent of delay and only dependent on thermal noise. Practically, the upper bound of cancellation was found to be 55 dB – the dynamic range of the VSA is only 55-60 dB. This value of cancellation was constant across delay. However, when the WARP board was used to test the same experiment, the cancellation fell as a function of delay and floored at around 35 dB. Phase noise was considered as a suspect for this observation since the phase noise in the VSA receiver is much lower than that of the WARP board. When the same analysis was performed for residual error including phase noise, it was found that the cancellation is dependent on delay. Thus, phase noise acts as a bottleneck for active cancellation.

Section 1.4. – Research goals.

As shown in previous literature, the cancellation operation is dependent on multiple factors such as precise modelling of RF cancellation delay lines, antenna placement, and training or preamble sequences that may not be common or standard amongst all communication protocols. Moreover, recalibration of the channel is needed and this is dependent on training sequences for active cancellation methods. Although this type of algorithm works for slow fading channels, it is not entirely a closed loop system in which the transceiver actively tracks the self interference to adapt to any changes. With a closed-loop system, processing is constantly performed, implying that such a system is real-time and online.

The aim of this research is to prove that the Least Means Squared (LMS) algorithm works as a real time solution for echo cancellation. We will show that adaptive cancellation is achievable with the LMS algorithm and that it can be used in other realms such as RF or analog baseband for cancellation. A digital LMS cancellation method is implemented using a full duplex transceiver and a computer control system. The system was designed to conform to WiFi 2.45 GHz PHY standards. The maximum bandwidth achievable is 6.25 MHz.

Chapter 2 discusses multipath and the design information about the transceiver, Chapter 3 describes the LMS implementation and adaptive cancellation, and Chapter 4 contains the results of the tests including all functionality tests of the board. Finally, Chapter 5 will conclude the experiment.

CHAPTER 2

FULL DUPLEX FRONT-END DESIGN

Section 2.1. – Mathematical model of the received signal

Component non-linearity, noise, and multi-path effects corrupt the TX signal before it interferes with the RX path. Therefore, one cannot trivially subtract the TX signal from the RX signal without processing it first. The transmitted baseband signal can be represented as:

$$TX_{baseband}(t) = I(t) + jQ(t) \quad \textbf{(1)}$$

$$= \sqrt{I^2 + Q^2} e^{j*\text{atan}\left(\frac{Q}{I}\right)} \quad \textbf{(2)}$$

$$= A(t)e^{j\phi(t)} \quad \textbf{(3)}$$

This signal represents any generic quadrature modulation scheme. After upconversion to RF, we have:

$$TX_{RF}(t) = A(t)\cos\left(\omega_{RF}t - \phi(t)\right) \quad \textbf{(4)}$$

This signal is ideal and not affected by noise or distortion. After the signal is transmitted, it is corrupted by multipath before it reaches the receiver:

$$RX_{RF}(t) = \sum_{n=1}^{\infty} \alpha(n)e^{u(n-1)j\Phi(n)}A(t - t_n)\cos\left(\omega_{RF}(t - t_n) - \phi(t - t_n)\right) \quad \textbf{(5)}$$

After downconversion, the resultant I channel baseband signal will be:

$$RX_{BB\_I}(t) = \cos(\omega_{RF}t)\sum_{n=1}^{\infty} \alpha(n)e^{u(n-1)j\Phi(n)}A(t - t_n)\cos\left(\omega_{RF}(t - t_n) - \phi(t - t_n)\right) \quad \textbf{(6)}$$

$$= \sum_{n=1}^{\infty} \alpha(n) e^{u(n-1)j\Phi(n)} A(t - t_n) \cos\left(\omega_{RF} t - \omega_{RF}(t - t_n) - \phi(t - t_n)\right) \quad \textbf{(7)}$$

$$= \sum_{n=1}^{\infty} \alpha(n) e^{u(n-1)j\Phi(n)} A(t - t_n) \cos\left(-\omega_{RF} t_n - \phi(t - t_n)\right) \quad \textbf{(8)}$$

The Q channel will be:

$$= \sum_{n=1}^{\infty} \alpha(n) e^{u(n-1)j\Phi(n)} A(t - t_n) \sin\left(-\omega_{RF} t_n - \phi(t - t_n)\right) \quad \textbf{(9)}$$

If the transmitted constellation looks like graph in Figure 2.1, the received constellation, without delay phase rotation, will look like the graph in Figure 2.2.

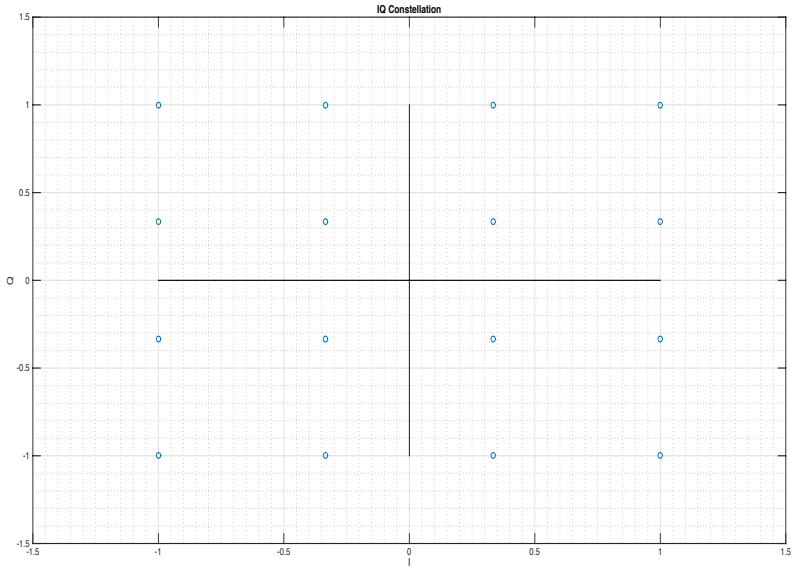

Figure 2.1 – Transmitted 16QAM constellation

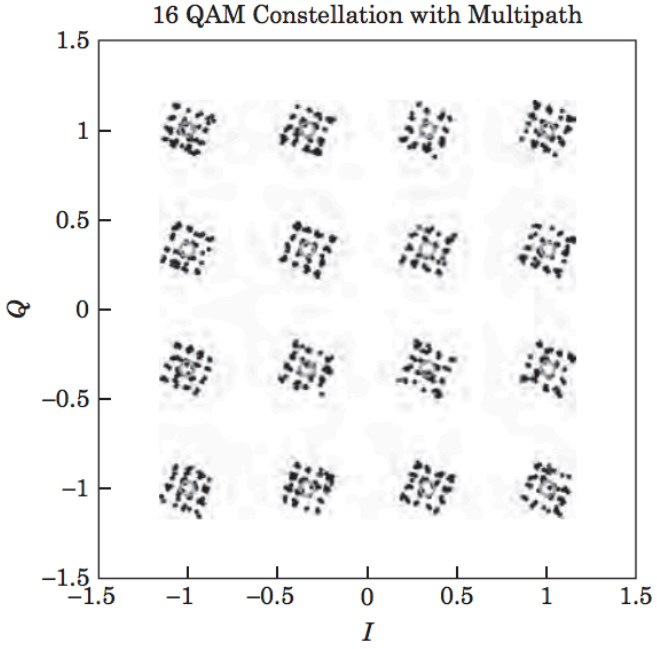

Figure 2.2 – Received signal after corruption by multipath [9]

The strongest signal will be captured by the receiver and will lie in the nominal constellation point (albeit rotated by $\omega_{RF}t_1$). The remaining attenuated multipath signals will be captured around the main constellation point. Each one of this miniature constellation clusters will rotate themselves based on what the channel environment and relative time delay is like.

The system will have to create multiple delayed copies of the TX signal to successfully cancel out the self-interference signal and other multipath signals. The non-linearity of the TX path can be modeled using a polynomial expansion, however, this will be skipped here. To realize the full-duplex experiment, a test transceiver board was created. The WARP platform was initially considered but a custom design was chosen for improved bandwidth and increased access points in the baseband and RF section.

Section 2.2. – System board front-end design

To implement a full duplex system with multiple tap points and cancellation options, a board was created with two transceiver chains totaling four RX/TX paths in total. An LO of 2.45 GHz is used for this experiment. The system was designed for the WiFi PHY. Figure 2.3 shows a top-level system block diagram of the board.

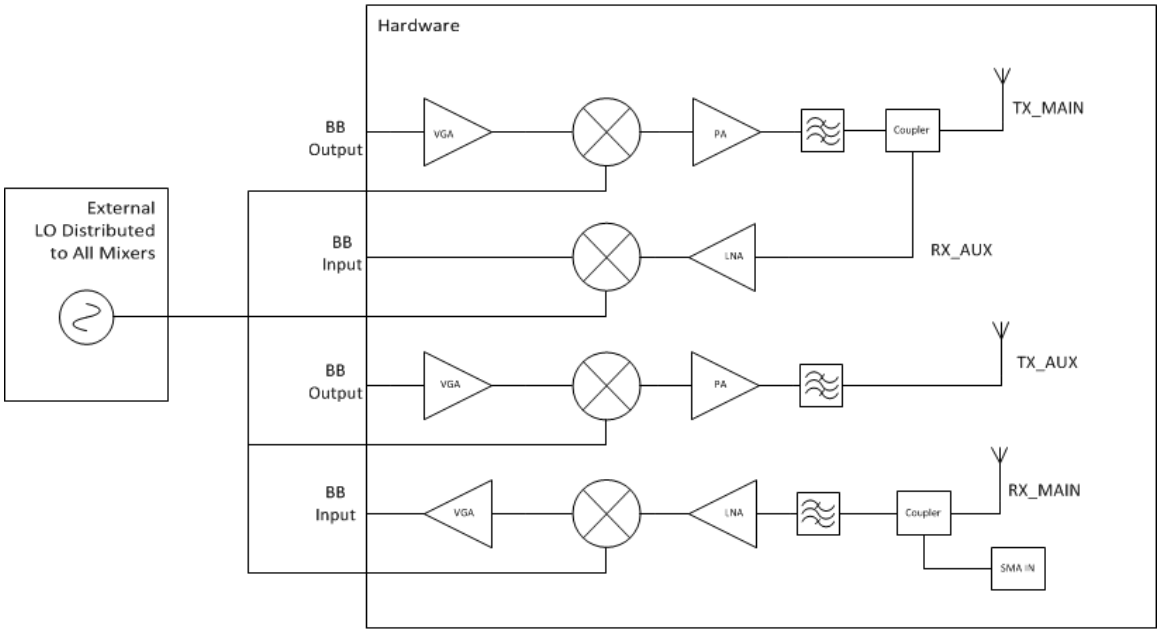

Figure 2.3 - Top level system diagram

The auxiliary RX chain is used to down convert the TX signal directly from the near the antenna using a directional coupler. This removes any multi-path phenomenon caused by the channel and preserves the non-linearity created by the TX components. Because the same Local Oscillator (LO) is used for the TX and RX paths, the LO phase noise will be correlated and removed. This signal can be run through several complex filters that introduce delay and injected into the main baseband RX chain.

The auxiliary TX chain is used to inject an RF signal directly into the main RX path just before the SAW BPF channel filter. Since this method includes the same TX

components placed at the same distance, the signal will be affected the same – however, the non-linearities do vary from component to component and the thermal noise will not be correlated. The main TX channel will of course be used to transmit actual data to another wireless receiver. Finally, the main RX channel will be used to demodulate incoming signals from another wireless transmitter.

The main RX channel has two injection points for the cancellation signals: at RF before the SAW BPF and in the analog baseband domain just before the VGA. A coupler is used at RF to inject the cancellation signal and a resistor network with DC blocking capacitors is used in baseband. The following section will present a low-level system block diagram and describe the component level design of the board.

Section 2.3. Component level board design

The component block diagram is shown in Figure 2.4. The 2 TX and 2 RX channels are connected to external ADCs and DACs. For this particular experiment, only one DAC and ADC were used. This will be expanded on later in the system implementation section. All other components are integrated onto a PCB and routed manually. The schematics will now be explained in detail. All schematics were designed using OrCAD Capture and the board layout was designed in OrCAD PCB Editor.

The first block in the TX section is the Variable Gain Amplifier (VGA). To filter out any residual quantization noise and ensure that the transmitted signal remains in band, a low pass filter should be employed before the upconverting mixer. A suitable VGA was found that contains both an integrated filter and a programmable gain (both through analog and through a SPI interface).

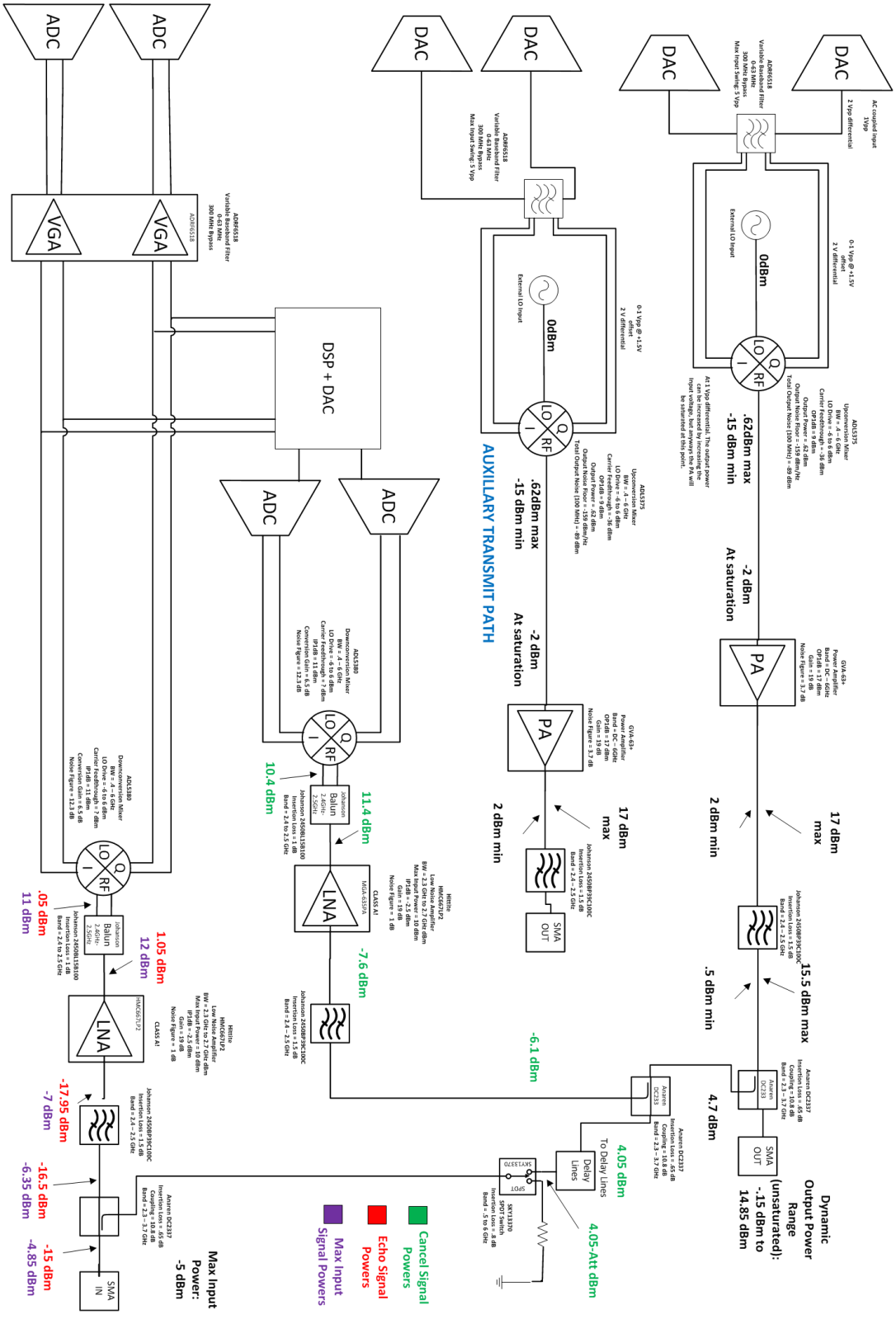

Figure 2.4 - System component level block diagram

The VGA chosen is the ADRF6518 and the schematics for this component are shown in Figure 2.5. The input is connected from the external two channel DAC (not shown) through a SMA to U.FL connector. These are then fed through DC blocking capacitors and a bias network to the input of the VGA. The ADRF6518 can either provide its own bias or have a bias be produced externally. The bias resistors footprints were included in case the DC blocking capacitors needed to be removed for any reason. The enable pin is set using an off page resistor divider. The power supply is filtered using several bypass capacitors. The multiples of capacitors were placed in the schematic so that they could be physically located near the multiple power pins in the chip. The gain of the amplifier is controlled using three pins set between 0-1 V. The amplifier actually consists of three amplifiers in series as shown in Figure 2.6.

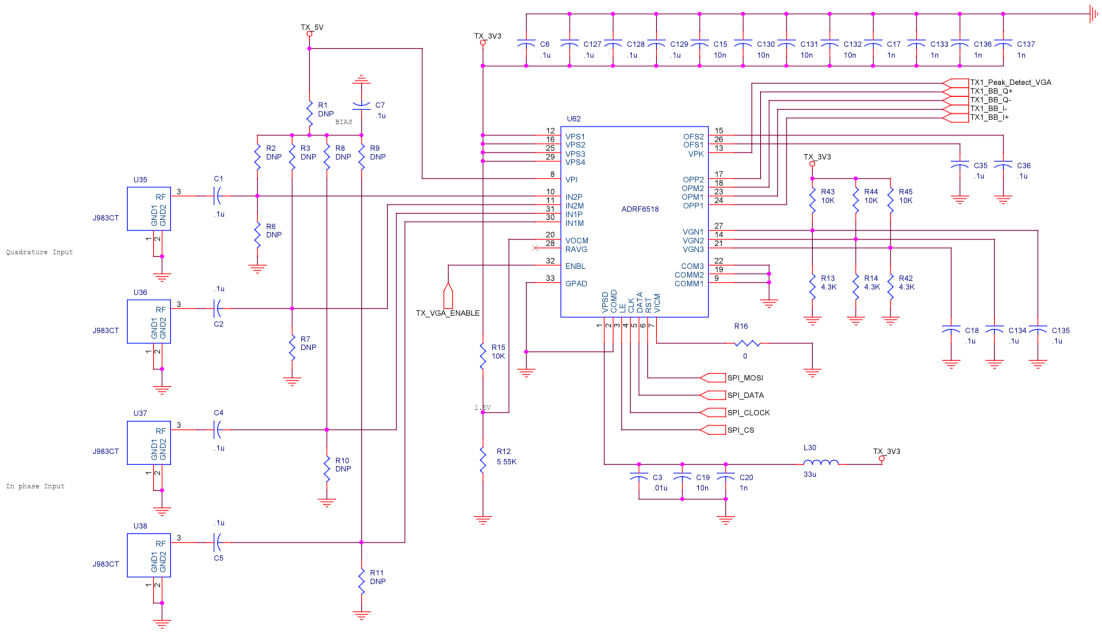

Figure 2.5 - TX VGA schematic

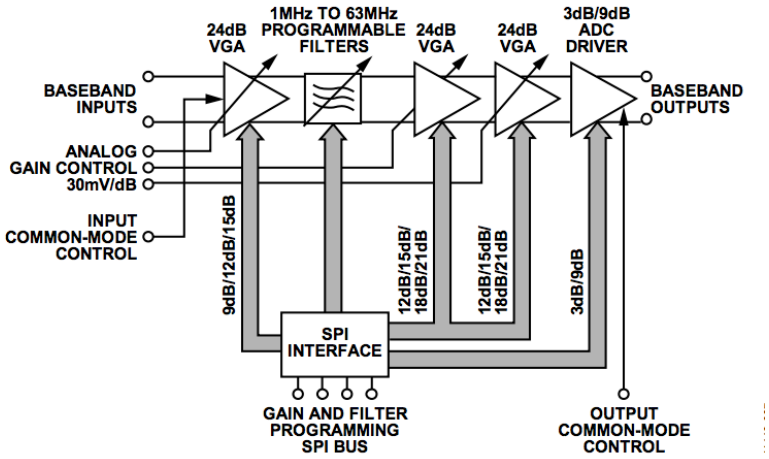

Figure 2.6 - VGA internal architecture

For maximum linearity, the gain of the first two amplifiers should be set low and only the third amplifier gain varied. However, for small signal inputs, the gains can all be set as high as possible to reduce the noise figure and maximize the gain of the VGA. The ADRF6518 also contains a variable low pass filter that ranges from 1 to 63 MHz The filter can be completely bypassed to 300 MHz after programming. A resistor divided voltage fed to a biasing pin controls the output common mode of 1.5 V (the required input common mode of the mixer). The same VGA is used for the RX chain – this schematic will be shown later. The specifications are shown below in Table 2.1.

Table 2.1 - VGA specifications

Agilent ADRF6518	Baseband VGA	Voltage Supply	3.15	3.3	3.45	V
		Current Supply	360		400	mA
		Bandwidth	1		63	MHz
		Output Noise		-104.6		dbV/Hz
		Max Output Load		400		Ohms
		I-Impedance Diff		400		Ohms
		DC Output Common Mode	0.9		2.1	V
		DC Input Common Mode	1.35		3.1	V
		Max V Gain		66		dB
		Min V Gain		-36		dB
		Logic - VIH		2		V
		Logic - VIL		0.8		V
		Logic - IIH		1		uA

The differential I and Q outputs of the VGA are then fed to the upconverting mixer. The ADL5375 was chosen due its wide bandwidth and simplicity. The mixer schematic is shown in Figure 2.7.

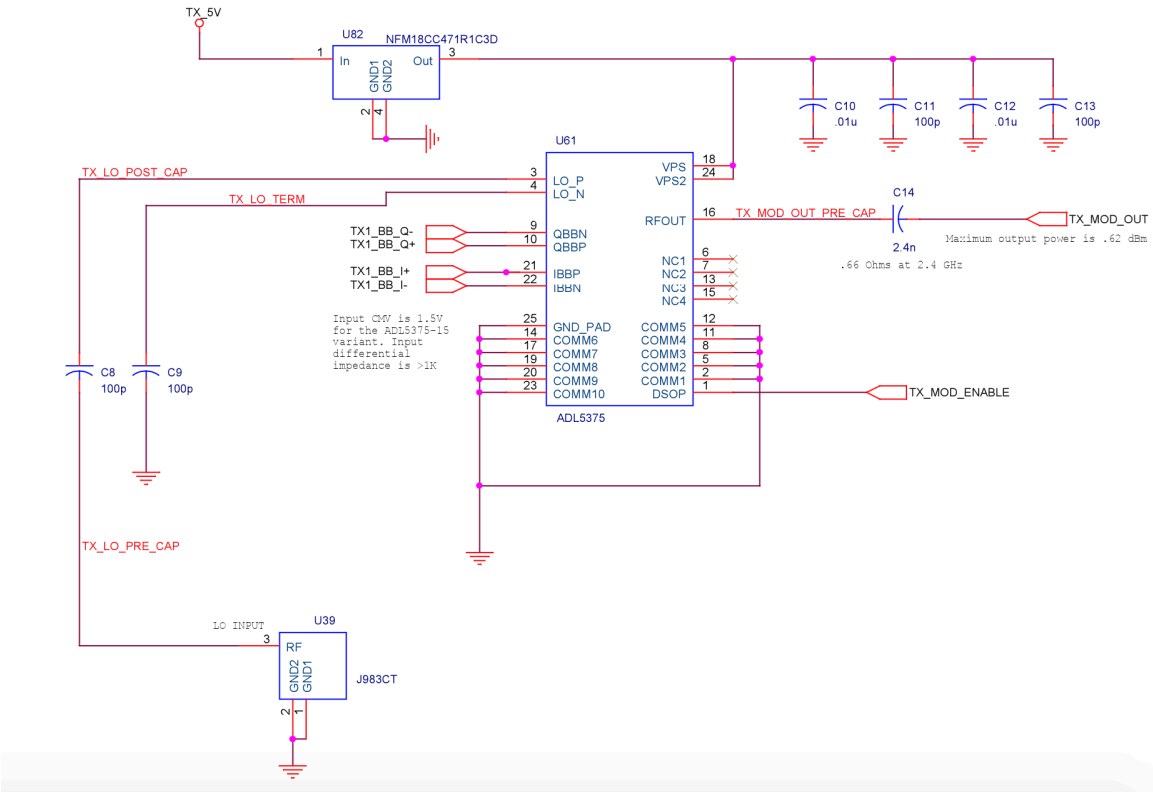

Figure 2.7 - TX mixer schematic

The LO is connected through a U.FL connector placed near the chip. The ADL5375 can be configured using a single ended LO if the other negative port is grounded using a capacitor. As long as the input common mode voltage is set properly and the output is DC blocked, no additional external circuitry is needed for operation. The power supply is bypassed with several capacitors and is fed through a DC coupling component to ensure a clean voltage. The mixer specifications are shown in Table 2.2.

Table 2.2 - TX mixer specifications

Analog Devices ADL5375	Upconversion Mixer	Voltage Supply	4.75	5	5.25	V
		Current Supply		194		mA
		Output P1dB		9.6		dBm
		Output IP3		22.7		dBm
		Output Power		0.61		dBm
		Noise Floor		-159		dBm/Hz
		LO Power	-6	0	6	dBm
		Input LO VSWR		< -10		dB
		Band	0.4		6	GHz
		I/Q Voltage (single)		1		Vpp
		I/Q Common Mode		0.5		V

The output of the mixer is then fed to a power amplifier. The GVA-63+ was used for this design. The P1dB of the PA is 17 dBm (at around 2.4 GHz) which is within appropriate WiFi power levels. The maximum power level for the WiFi PHY layer was set as the upper power limit for the design – however the lower limit was decided upon based on the components in the chain. The PA schematics are shown in Figure 2.8.

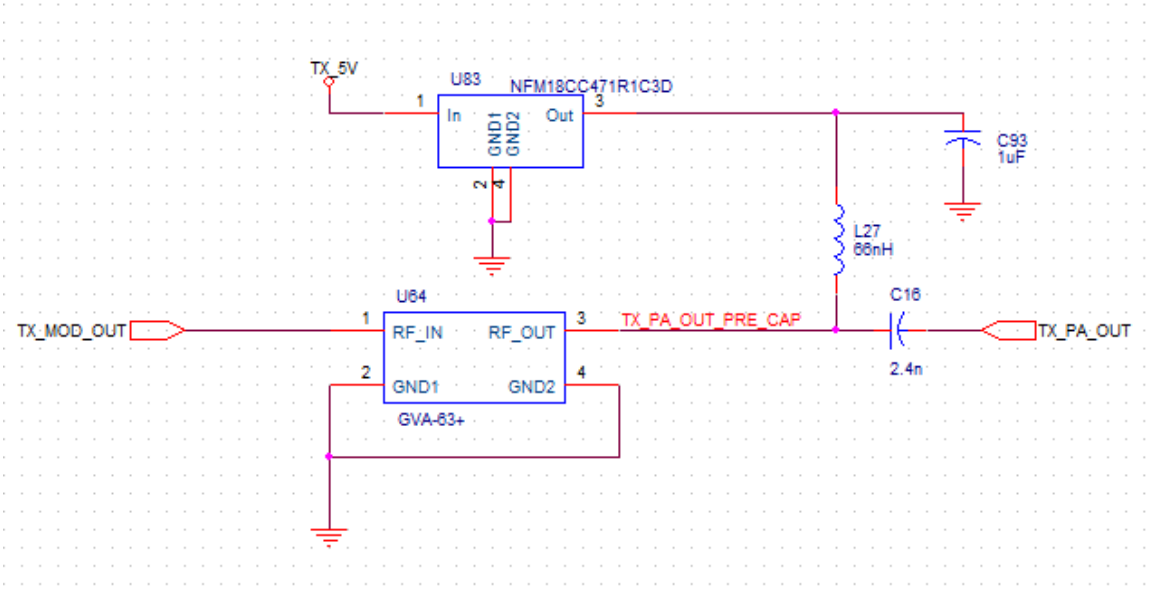

Figure 2.8 - TX PA schematic

The input is simply fed into the one pin on the chip (it has already been DC blocked from the previous stage). The output matching/biasing is provided using a network suggested by the GVA-63+ datasheet. The same DC coupling component is used to power the chip.

The final two components of the TX chain include the output WiFi PHY 100 MHz SAW BPF and the directional coupler to feed the signal into the auxiliary RX chain. This is shown in Figure 2.9 and 2.10.

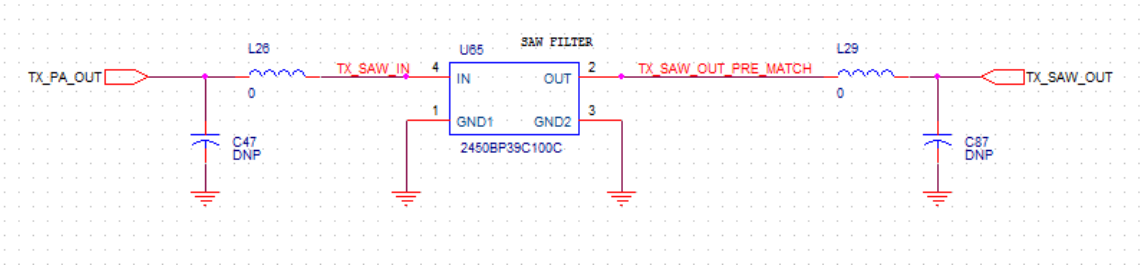

Figure 2.9 - TX SAW filter

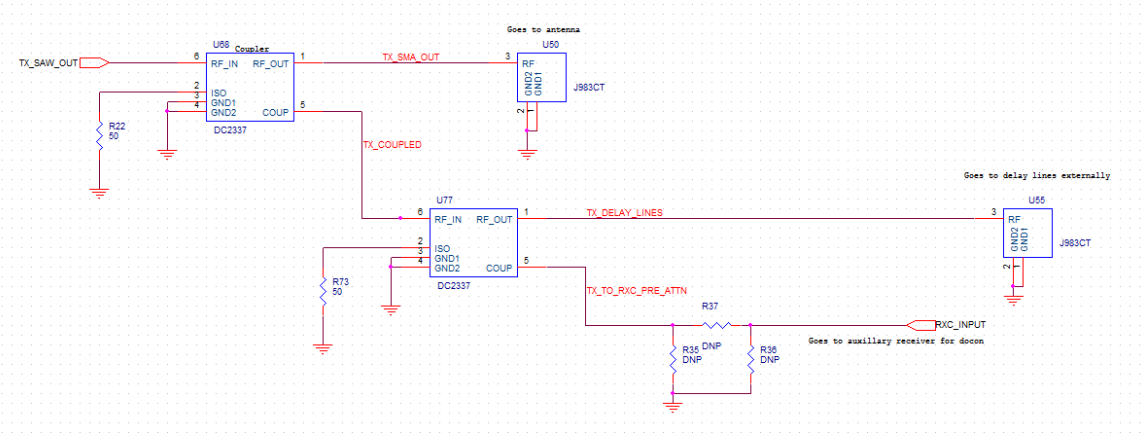

Figure 2.10 - TX output chain

Another directional coupler provides an access point for the RF cancellation lines. The theory behind how the cancellation works will be explained in Chapter 3. An attenuation network is provided between the TX and auxiliary RX to reduce the signal power to within the maximum IP1dB. The saturation point of the PA is around 17 dBm and the insertion loss of the SAW filter and coupler combined is 2.1 dB resulting in a total system output

saturation power of 14.9 dBm. This corresponds to an OIP3 of about P1dB + 10 dB = 25 dB. The auxiliary TX is a duplicate copy of the main TX chain with the exception of the directional couplers. The output is located directly after the SAW filter.

The RX chain uses the same SAW filter and directional coupler as the TX chain. This can be seen in Figure 2.11.

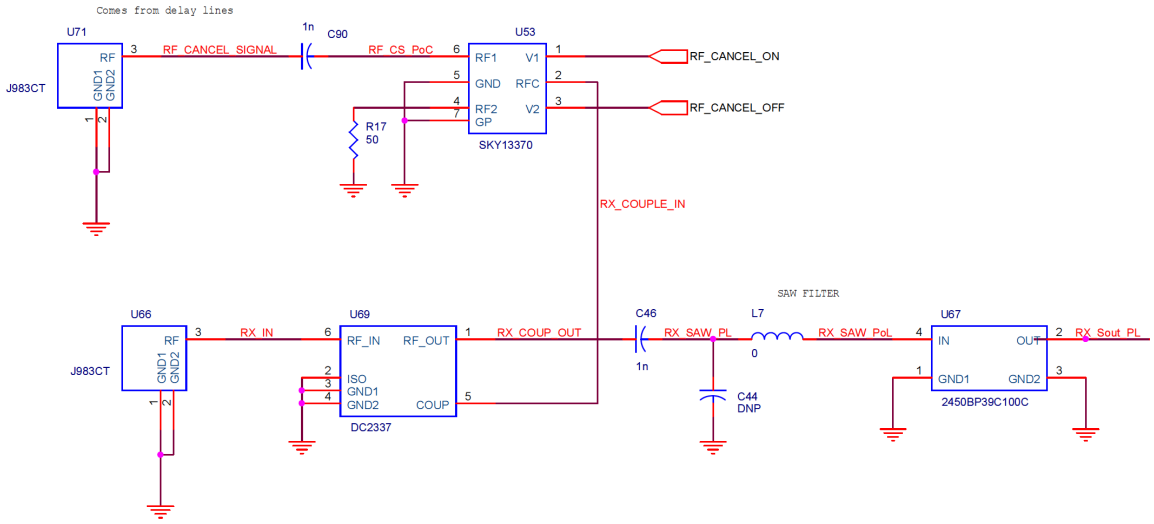

Figure 2.11 - Main RX input

An RF switch is included to provide the option of turning on or off the RF injection point. The RF injection point is coupled into the main RF RX path that is brought in using a U.FL connector. This connection passes through the 100 MHz SAW BPF filter and is fed into the LNA. The LNA schematic is shown in Figure 2.12 and the specifications in Table 2.3. The Hittite HMC667LP2 was used for the transceiver. The required LNA circuitry is minimal and the matching was chosen based on the datasheet recommendations. The voltage supply line was fed through a DC coupler just like all other active RF components on the board. Likewise, bypass capacitors were provided to further filter the power supply.

The output of the LNA is singled ended and thus a balun was inserted between the LNA and the downconverting mixer.

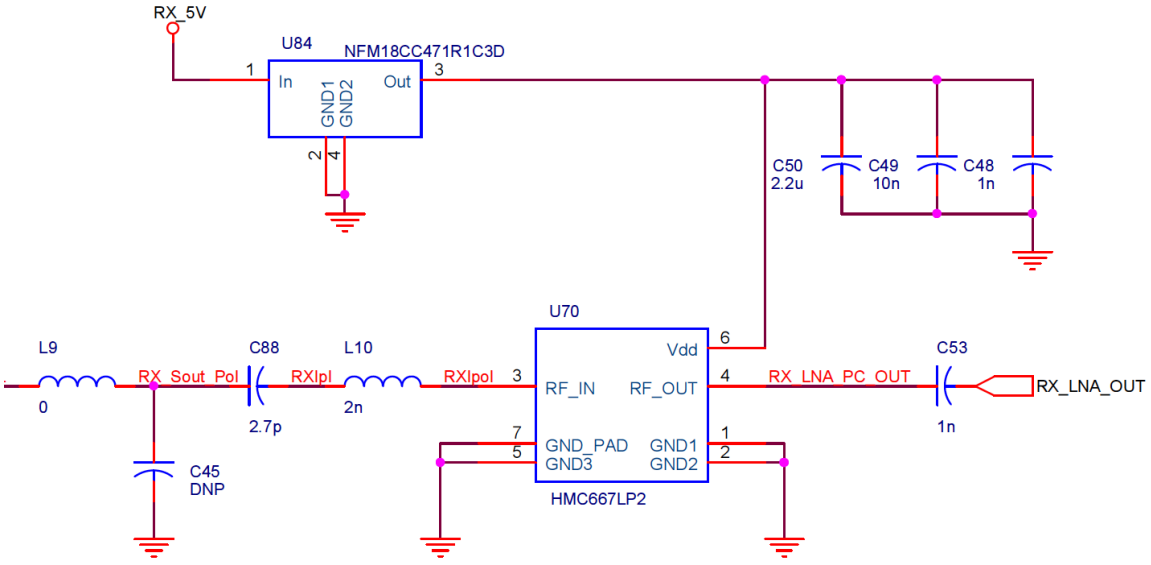

Figure 2.12 - LNA schematic

Table 2.3- RX LNA specifications

Hittite HMC667LP2	LNA	Voltage Supply		5		V
		Current Supply	59		75	mA
		Gain		19		dB
		OIP3		29.5		dBm
		NF	0.75		1.1	dB
		OP1dB		16.5		dBm
		IRL		-12		dB
		ORL		-14		dB
		S12				dB
		Max Input Power		10		dBm

The downconverting mixer schematic is shown in Figure 2.13. This also includes the balun. Similar to the ADL5375, the ADL5380 was chosen for its wide bandwidth and simplicity. The same DC coupler and bypass capacitors can be seen in the schematics. The LO for this component is also configured in the same single-ended connection like with the other chains.

The last component in the RX chain is the VGA. Unlike the TX VGA configuration that uses a set voltage to fix the gain at the output, the RX VGA configuration has variable gain ports controlled by either ADC control lines or potentiometers that are adjusted manually. This configuration allows an AGC loop to be implemented. The VGAs, however, are the exact same. The RX VGA's filter also acts as an anti-aliasing filter since the outputs are fed directly to the ADC. Moreover, the RX VGA contains analog injection points that allow analog cancellation signals to be added to the RX baseband signal. The gain control circuitry is shown Figure 2.14 and the input stage circuitry is shown in Figure 2.15. The overall RX VGA schematic is shown in Figure 2.16. The RX auxiliary chain does not include a VGA and the output is taken directly from the downconverting mixer.

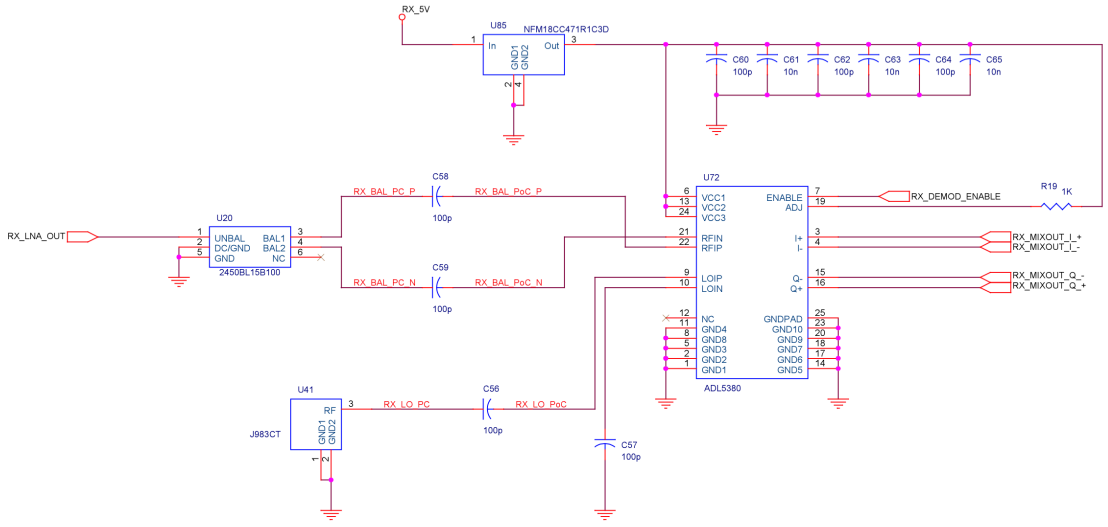

Figure 2.13 - RX downconverter mixer schematic

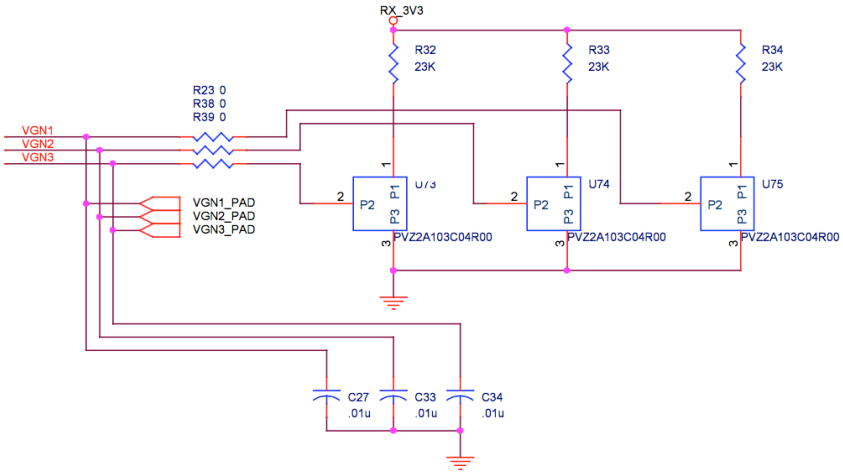

Figure 2.14 - RX VGA gain control circuitry

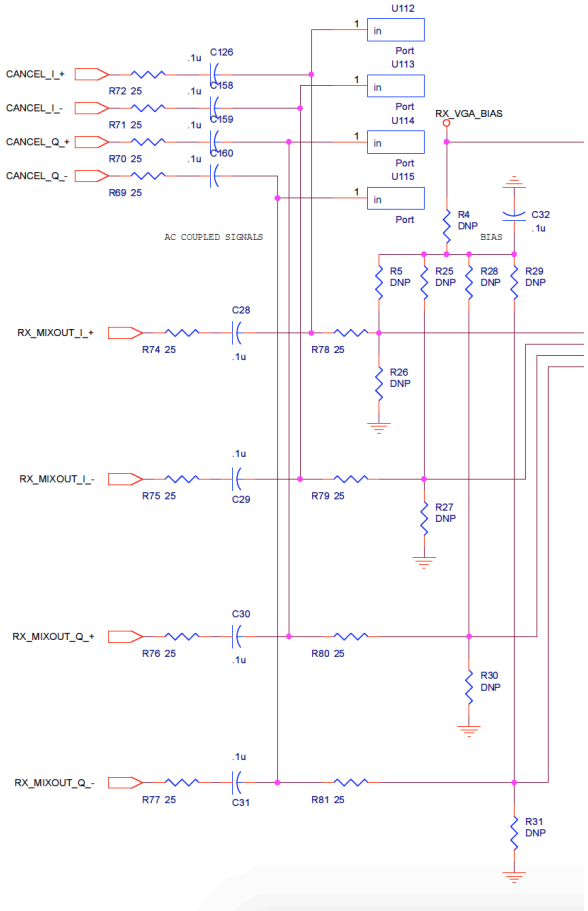

Figure 2.15 - RX VGA input stage

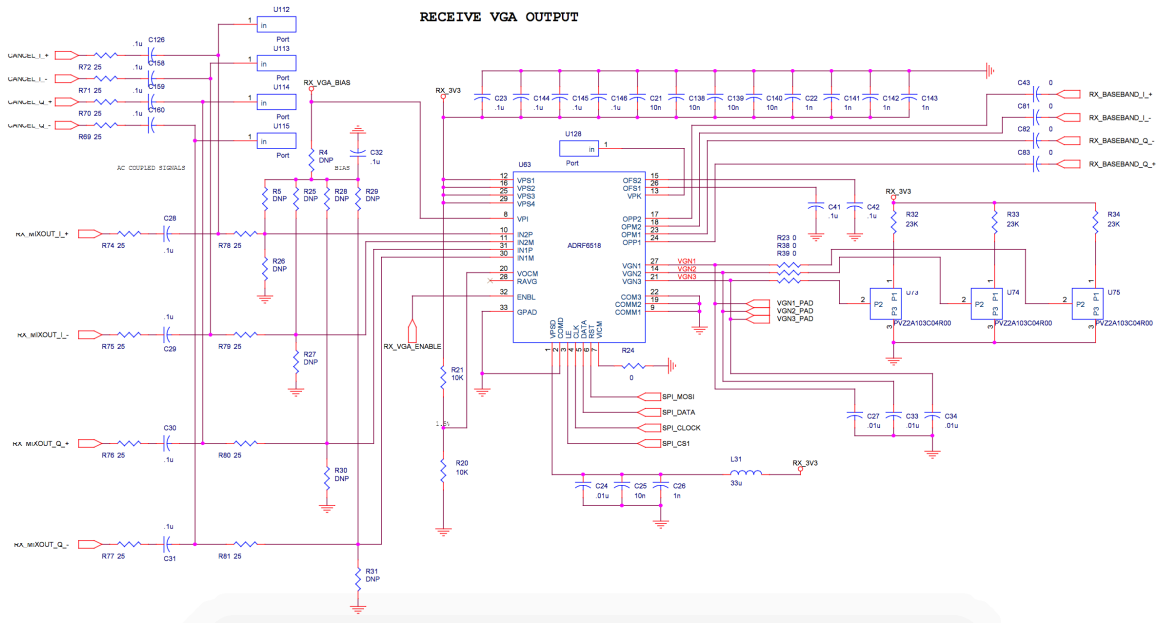

Figure 2.16 - RX VGA schematic

The power for all the chips is provided by individual Low Dropout Regulators (LDOs). Since the VGAs need both 3.3 V and 5 V and the other chips 5 V, two variants of the same regulator were included. The LT1117-3 and LT1117-5 were selected as viable candidates. The input voltage of the system was then set to roughly 6.5 V to provide adequate headroom for the dropout. Each power rail had an LED to indicate if the line regulator was on or not. The power supply generation schematics are shown in Figure 2.17 and 2.18.

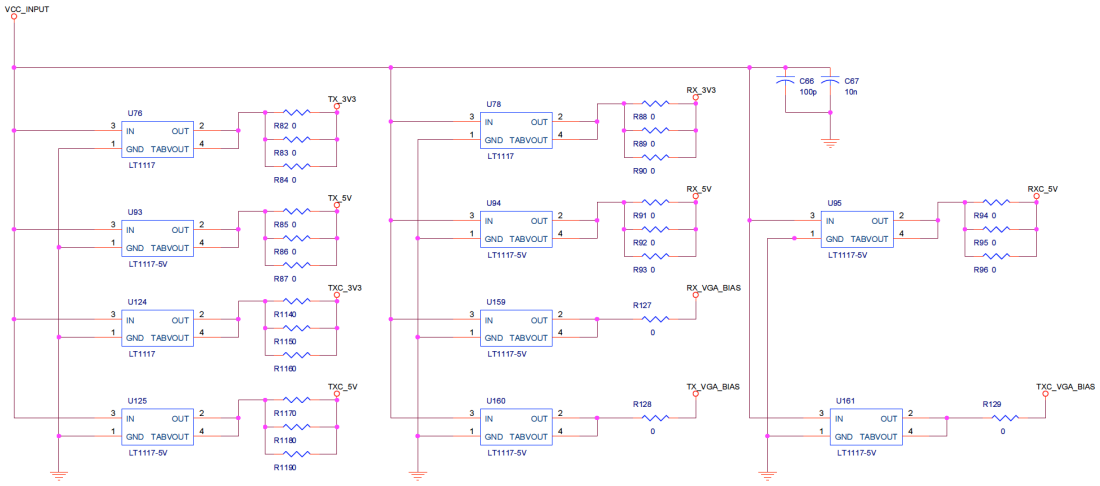

Figure 2.17 – Power supply generation schematics

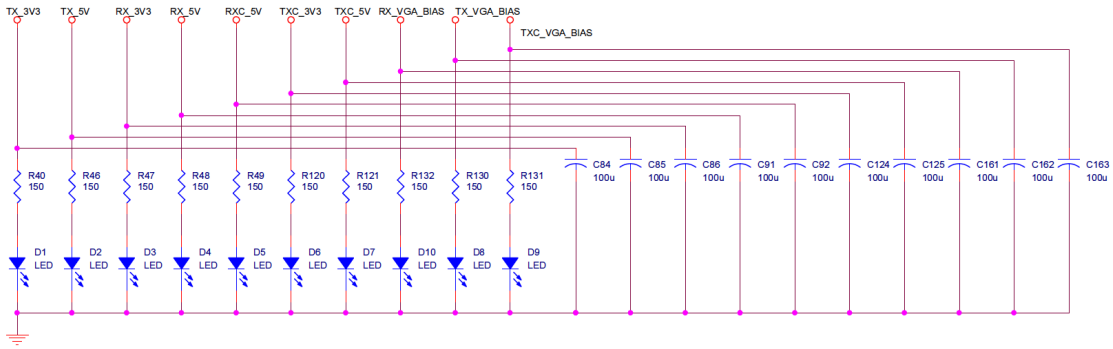

Figure 2.18 - LED power indicators

Each output was also bypassed to ground using a large capacitor with a value of 100 μF. In addition to the previous schematics, additional connectors and resistors were placed to bias the enable pins of the chips and to provide probe points for signals and voltages.

Section 2.4. – System integration

The integrated system diagram including the ADC and DAC and all connections is shown below in Figure 2.19.

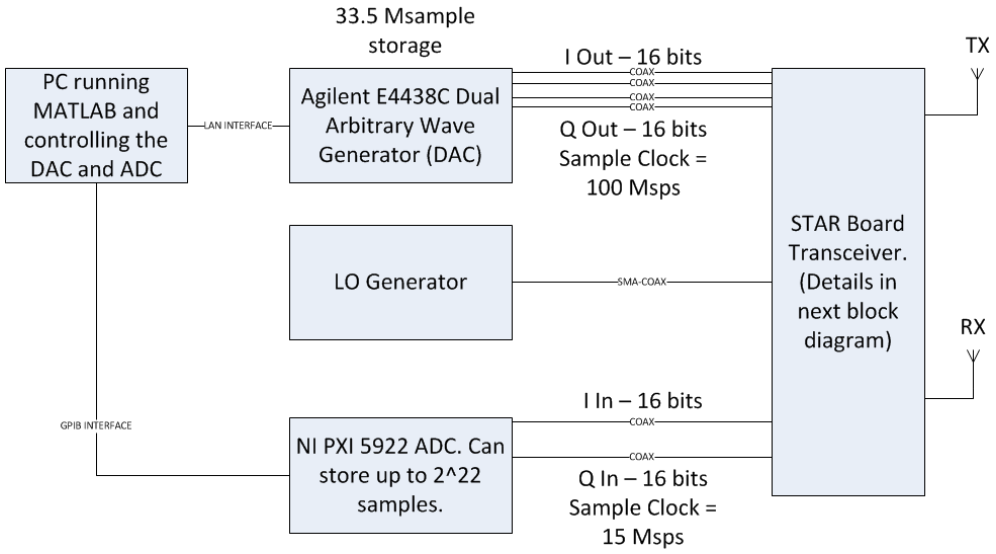

Figure 2.19 - Integrated system block diagram

The ADC and DAC are clearly more powerful than typical WiFi integrated radio digital acquisition components [1] however, for the sake of proving that the LMS algorithm works, they will suffice. The National Instruments PXI 5922 ADC was used as the ADC. It can be controlled using a PC through a GPIB connection. Either MATLAB or Labview can be used to program and acquire data. For this experiment, MATLAB was the sole processing tool because it was easier to integrate algorithm and control software. The ADC specifications are shown in Table 2.4.

Table 2.4 - ADC specifications

ADC Specification	Value
Max # of bits	24 (16 at 15 Msps)
Max Sample Rate	15 Msps
Full Scale Range	2V or 10V (2V is used)
On-board Memory	32 MB/channel
SFDR (at 1 MHz)	92 dBc

It must be noted that the ADC-MATLAB interface is not a real time process (it can be configured for real-time using a circular buffer, however, this was not done for this experiment). The results of this experiment can be considered pseudo real-time though if the algorithms and processing used were to be implemented on an FPGA, the system would then be considered real time. The ADC is used by first setting up a trigger edge/time and capture length. The ADC is then armed by initiating an acquisition (during which MATLAB will wait before advancing through the script). Once the acquisition is complete, data is acquired from ADC in one binary batch. This data is then processed sample-by-sample to emulate a real time environment.

The DAC used is the Agilent E4438C ESG Vector Signal Generator (VSG). This machine is capable of modulating differential I and Q baseband signals up to RF and concurrently outputting these signals through external ports. The RF is not used since the transceiver board is upconverting the baseband signals up to RF. The VSG is programmed using SCPI commands sent through MATLAB. Although the VSG is capable of generating pseudo-random binary sequences (PRBS) on its own, it is preferred that data is created in MATLAB since this TX data is needed for the LMS cancellation algorithm. The data created in MATLAB takes on some form of modulation including QPSK, 8PSK, and 64QAM. A random stream of bits is mapped to each constellation point and these symbols are then upconverted to the specified sample rate of the DAC. The data is run through a root raised cosine pulse-shaping filter that smears the data in the time domain while concurrently avoiding Inter-Symbol Interference (ISI). After the data is created in MATLAB, it is converted to unsigned 16 bit integer data and written as one binary block to the VSG. The trigger setup is then programmed in and the machine is set to repeatedly

send a single burst of data every time a trigger is received. Because the data is pseudo-random and essentially white noise in the frequency domain, the same data can be repeatedly sent without loss of generality with respect to the cancellation experiment. The DAC and ADC use the same trigger so the data sent out is immediately captured. The DAC specifications are shown in Table 2.5.

The same LO is used for both TX and RX which means that this system is a Zero Intermediate Frequency (ZIF) or homodyne architecture. The advantage of this is that phase noise is correlated, and there is no image to worry about (as is the case with a non-zero IF or heterodyne architecture). Furthermore, selectivity of the receiver is increased and Adjacent Channel Power Ratio (ACPR) becomes less of a problem since the receiver is more precise than a heterodyne one. However, the one major disadvantage of a homodyne receiver is the presence of DC offset if LO leakage and self-mixing occurs. This can theoretically be mitigated with large DC blocking capacitors, however, energy at lower frequencies may be lost thus resulting in a degraded SNR.

Table 2.5 - DAC specifications

DAC Specification	Value
Max # of bits	16
Max Sample Rate	100 Msps
Full Scale Range	2 V
On-board Memory	36MB
SFDR	80 dB

With the DAC, ADC, LO, and transceiver board all finalized and designed, the system was integrated using coaxial cables and RF compatible U.FL cables. Two antennas with an isotropic gain of 2.1 dBi (monopole antennas) were used for the TX and RX and were placed at roughly 20 cm apart. The DAC is controlled by MATLAB through LAN and the ADC through GPIB. We will now cover the LMS algorithm used for cancellation and provide simulation results followed by the practical system implementation.

CHAPTER 3

ADAPTIVE BASEBAND INTERFERENCE CANCELLATION

Section 3.1. – Working principle of adaptive cancellation using the LMS algorithm

The LMS algorithm is one of the simplest adaptive filters that can be implemented. It essentially tries to match two signals together using a process that updates the coefficients of the FIR filter per iteration. Because the LMS algorithm operates on an iteration per sample basis, the algorithm can be considered on line and real time. Each sample taken in by the ADC is processed by the algorithm and the coefficients are subsequently updated. The LMS algorithm block diagram is shown below in Figure 3.1.

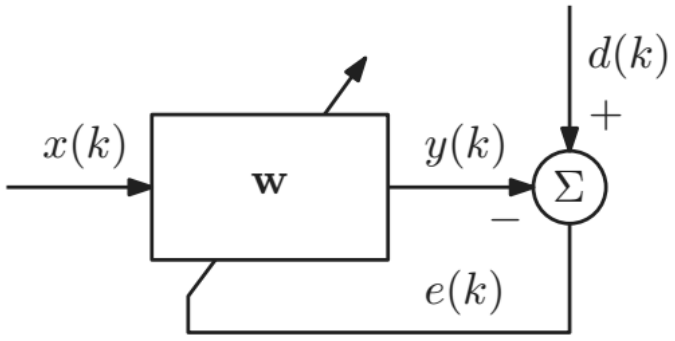

Figure 3.1 - LMS algorithm block diagram

The signal x(k), in this experiment, is the transmitted signal. Keep in mind that each 'k' represents one sample from the ADC. The adaptive FIR filter coefficients are represented by the vector **w** whose length is determined by the number of taps in the filter. The signal y(k) is the predicted receive signal which is subtracted from the actual received signal d(k). The LMS algorithm tries to force e(k) to 0 while concurrently updating the coefficients.

Mathematically, we can represent the predicted received signal as:

$$y(k) = \boldsymbol{w}^T \boldsymbol{x}(k) \tag{10}$$

where

$$\boldsymbol{w}^T = [w(k)\, w(k-1) \ldots w(k-N)] \tag{11}$$

and

$$\boldsymbol{x}^T(k) = [x(k)\, x(k-1) \ldots x(k-N)] \tag{12}$$

in which N is the number of taps in the FIR filter. The predicted receive signal is

$$y(k) = w(k)x(k) + w(k-1)x(k-1) + \cdots w(k-N)x(k-N) \tag{13}$$

and for the non-causal FIR case like in [1]:

$$\begin{aligned} y(k) = w(k+N)x(k+N) + w(k+N-1)x(k+N-1) \\ + \cdots w(k-N)x(k-N) \end{aligned} \tag{14}$$

Each error signal, for a causal at iteration k is represented by:

$$\begin{aligned} e(k) = d(k) - w[(k)x(k) + w(k-1)x(k-1) \\ + \cdots w(k-N)x(k-N)] \end{aligned} \tag{15}$$

The coefficients of the FIR filter are updated according to the following algorithm that uses the steepest-descent method:

$$\boldsymbol{w}(k) = \boldsymbol{w}(k-1) + \frac{\mu}{2}\nabla_{\boldsymbol{w}}\xi(k) \quad \textbf{(16)}$$

The scale factor μ sets the step size in each iteration. If the step size is too large, the feedback loop may become unstable – however, a larger scale factor will result in a faster convergence time which will allow the algorithm to correct for faster fading channels. $\nabla_{\boldsymbol{w}}\xi(k)$ represents the gradient vector of the mean squared error signal vector. A solution of this gradient is what is known as the Wiener solution. This requires knowledge of the auto correlation matrix of the input signal and the cross correlation matrix between the input signal and the reference signal. It also requires an inverse matrix transformation that makes real time implementation difficult. This gradient vector can be estimated by:

$$\boldsymbol{w}(k) = \boldsymbol{w}(k-1) + \mu\boldsymbol{e}(k)\boldsymbol{x}(k) \quad \textbf{(17)}$$

where e(k) was defined in Equation 15.

Section 3.2. – Adaptive cancellation system implementation

With the algorithm defined, the system cancellation was implemented as shown in Figure 3.2.

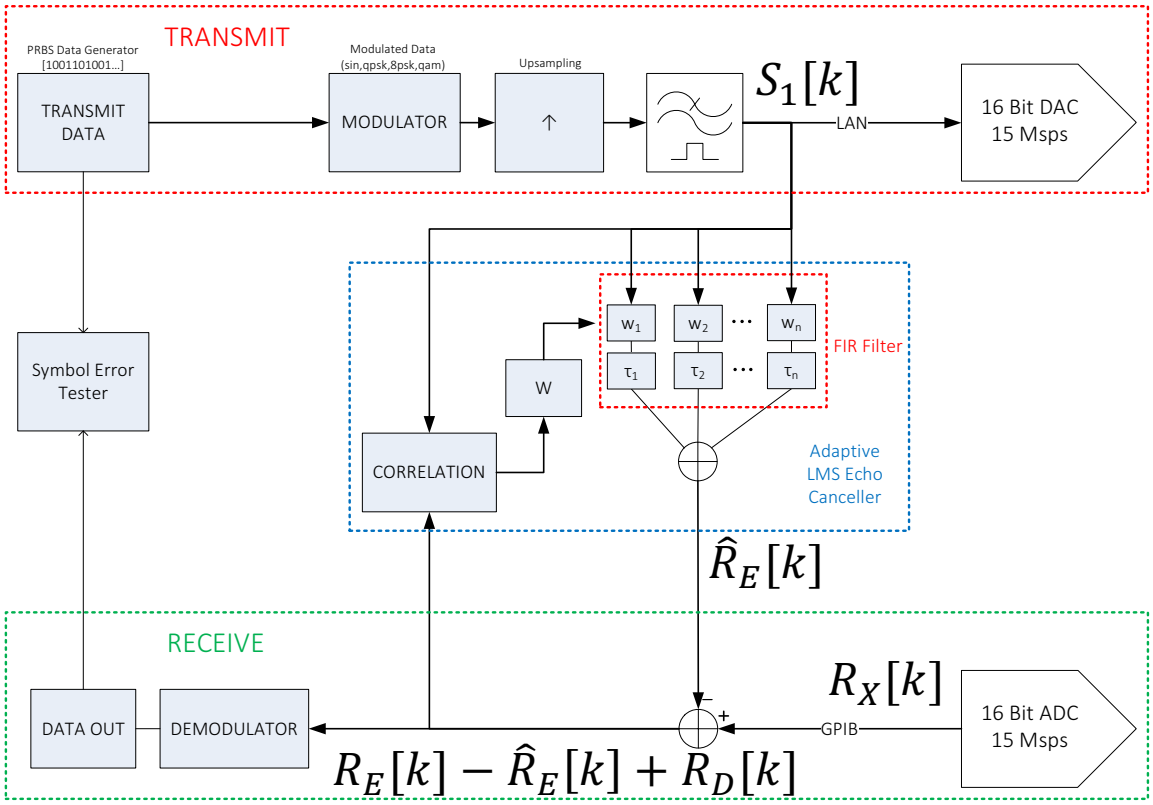

Figure 3.2 - System implementation with the LMS algorithm

The TX signal at baseband is tapped directly after the pulse-shaping filter and is fed to the FIR filter. If the filter is in non-causal mode, the delay of the system is adjusted such that the first tap delay is less than that of the channel delay. Note that an algorithm inside (similar to work in [8]) performs a coarse delay correction using complex valued cross-correlation functions that corrects for the main signal path delay. The LMS algorithm operates on the data on a sample per sample basis after each packet of data has been sent. Because of this operation, the system can be considered adaptive. It does not rely on any preamble or training sequence and is constantly updating with each and every sample.

The error signal e(k) is then fed into the demodulator. It should be noted that if the desired receive signal and the transmitted signal are correlated at any point in time, the BER performance will be diminished. The demodulator used in this project is a maximum likelihood detector with no forward error correction. This will provide the best result for a simple communication system and will suffice for this project. We must also mention that the transmitted signal itself is used to correct the phase/delay/amplitude of the desired received signal. This is an ideal case for this project – in practical implementations the transmitted data is completely unknown to the receiver and pilot tones are sent out with the data to provide information for automatic phase control. A preamble or 'start code word' will then typically signal the beginning of a packet. The demodulator block diagram is shown below in Figure 3.3.

A normalization block will first adjust the magnitude of the received signal to the transmitted signal. This is not really necessary (as will be seen later when discussing the decoder); however, it helps for debugging purposes. After this action is completed, the delay between the TX and RX needs to be corrected. This delay is the result of overall system delay and filtering and not the RF delay. This is done using a cross correlation function in MATLAB. After the delay correction operation, the phase needs to be corrected. The received constellation is rotated by the angle ωt_d where t_d is the time taken from the transmitter to the receiver in the RF domain. To correct for the phase, a one tap LMS algorithm is used to compare the transmitted and received signals. Only one tap is needed since we are trying to multiply the entire packet by a single complex value to rotate the constellation back to its original angle. The mean of the phase of the LMS coefficient

is then multiplied by the received signal. There are methods of performing this action that involve training symbols that were not used for this experiment.

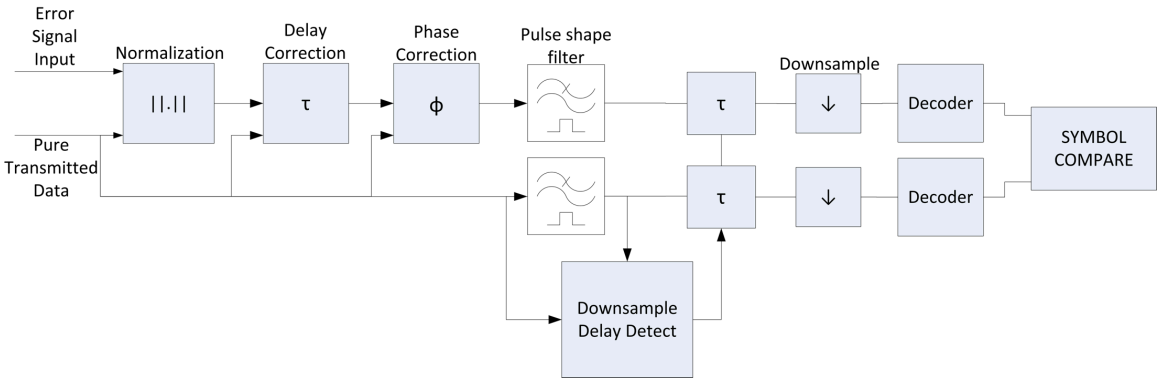

Figure 3.3 - Demodulator block diagram

After the phase correction, the signals are passed through a matched pulse-shaping filter to recover the signals. Several zeros are padded onto the beginning and the end of the sequence and therefore the ideal down sampling point needs to be adjusted for in the received signal. As stated before, the TX signal has been optimized for this so this signal is cross correlated with the filtered signal and the found delay is applied to both the TX and RX signals. This delay is not associated with the system or with the RF delay, rather, it is caused by the filtering and processing in MATLAB. These signals are subsequently down sampled and passed through the decoder. The decoder analyzes the Euclidian distance between the input symbol and each ideal constellation point and chooses the point with the minimum distance. It then assigns a symbol based on the symbol-alphabet mapping and assigns the symbols to an output vector. The TX and RX vectors are then compared to calculated symbol error rate.

Section 3.3. –Simulation Results

To test the LMS algorithm a sample signal is created in MATLAB using a PRBS sequence of 1000 bits at 1 Msps. As an example, Figure 3.4 shows what a pulse shaped constellation for an 8PSK modulation scheme will look like.

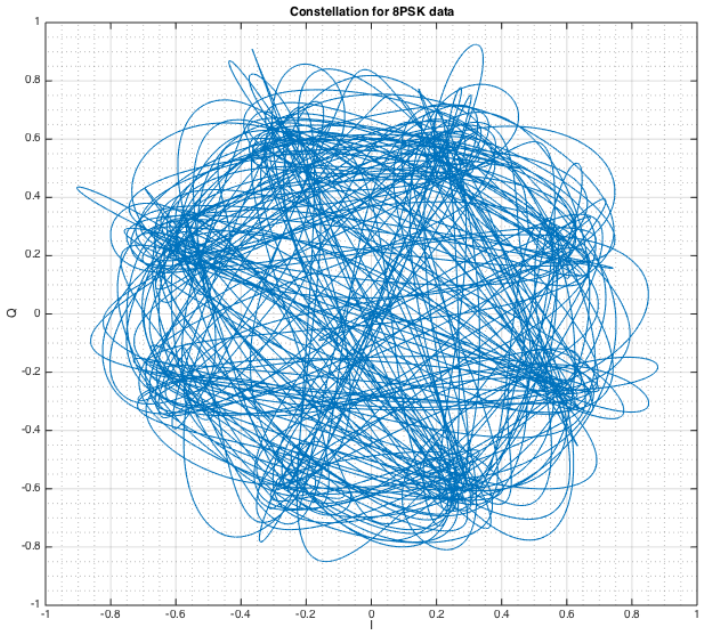

Figure 3.4 - MATLAB generated pulse shaped 8PSK constellation

For these experiments, no gray coding or any type of Forward Error Correction (FEC) was used. The symbol mapping is a simple linear relationship between the binary code and the symbol e.g. '000' would be symbol '1' and '111' would be symbol '7'. The spectrum of this data is shown in Figure 3.5.

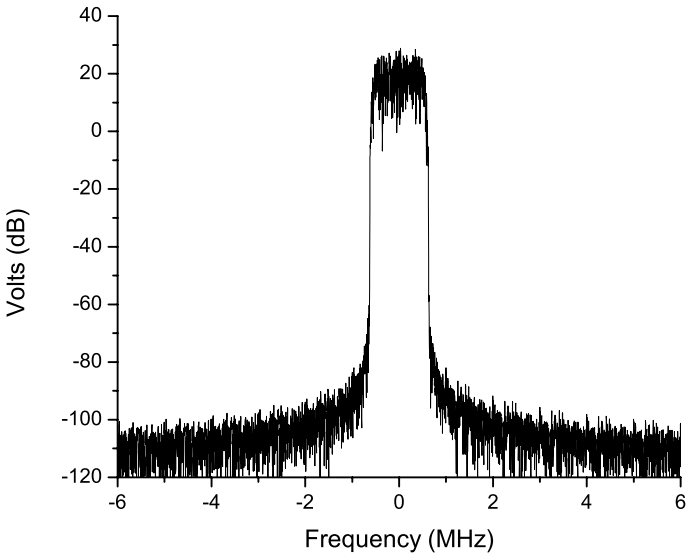

Figure 3.5 - Spectrum of the PRBS 8PSK data with a 1Msps symbol rate

The transmitted symbols are then rotated and delayed based on a simplistic channel model. The LMS algorithm is then deployed on the received symbols on a sample-by-sample basis. The magnitudes of the coefficients are shown in Figure 3.6.

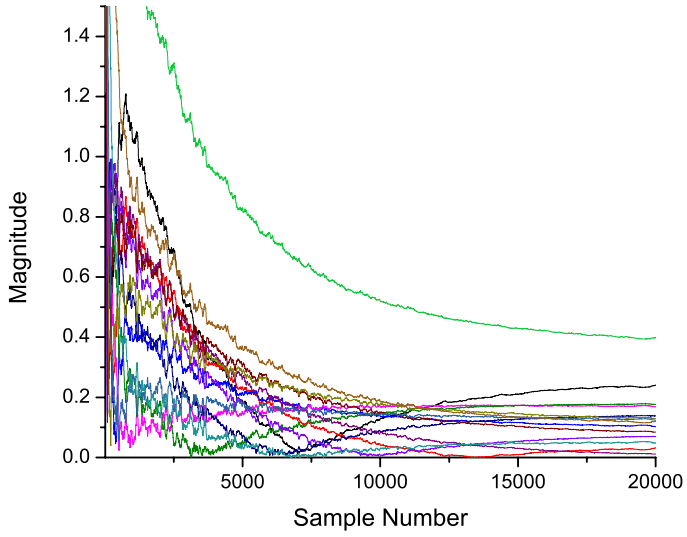

Figure 3.6 – Magnitudes of the LMS coefficients

The coefficients clearly converge after about 20000 samples or an equivalent time of 1.3 ms. The convergence time depends on the scale factor μ and increasing this too much may cause the system to become unstable. The time domain signals are shown in Figure 3.7 with the received signal and the error signal. Note how the error signal converges towards zero after roughly 20000 samples. The predicted signal starts tracking the received signal at this point.

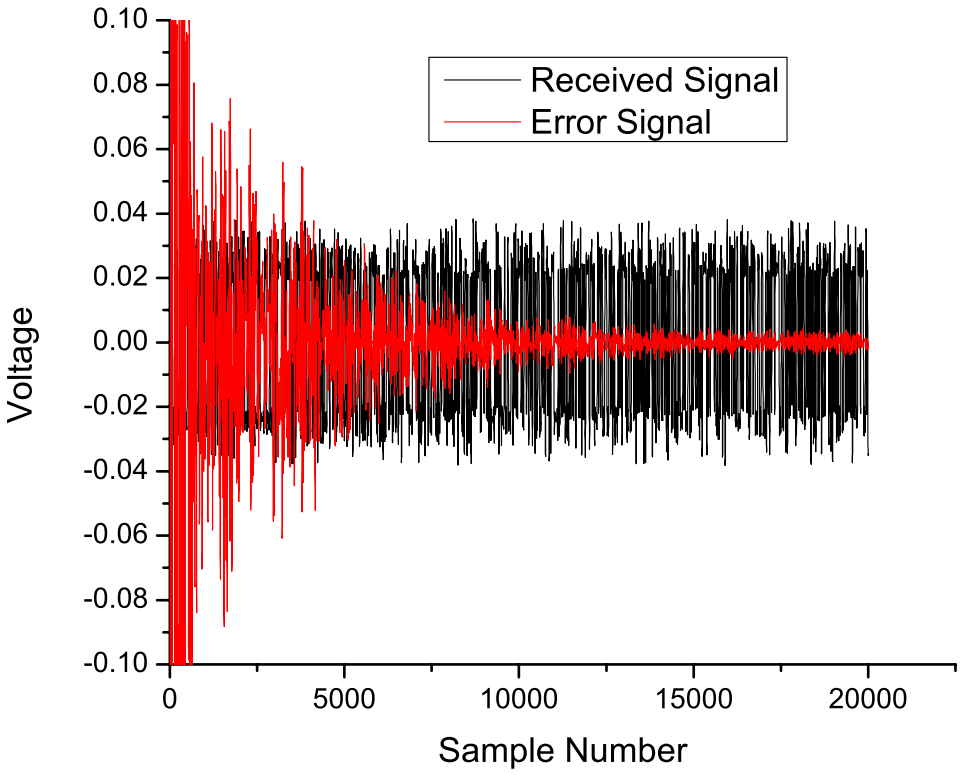

Figure 3.7 – The received signal (black) and the error signal (red).

If we look at the spectrum of signals that have been processed in a channel devoid of multipath and noise in Figure 3.8, we can see that the received signal is cancelled out to the MATLAB quantization noise floor. This is because neither multipath nor any other interference exists except for the actual data that the transceiver is trying to receive. A

cancellation of 162 dB can be obtained with this channel model – this is meaningless for any practical application, however, we now know that the LMS algorithm is functioning correctly. The calculated BER is 0 - at this point, only the Gaussian noise of the channel for the received signal will affect the BER. We must also note that any multi-path or fading effects of the received signal have been ignored since demodulation of these types of signals is beyond the scope of this project.

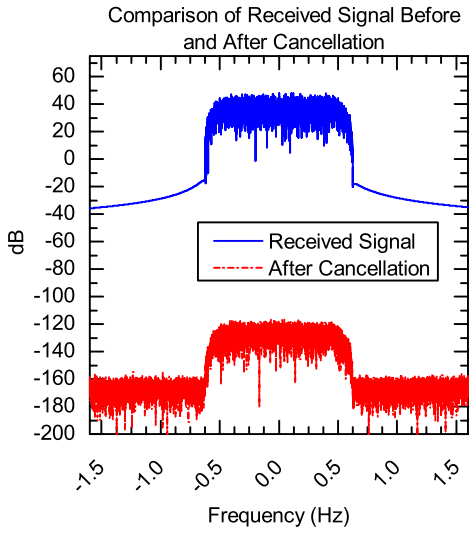

Figure 3.8 - Comparison of the received signal and the signal after cancellation. The cancellation is near perfect for a simple channel in which neither multipath nor delay exists. Note that the scale is relative.

If we now include multipath and apply it to the transmitted signal, we observe in Figure 3.9 that cancellation with only one tap won't nearly provide as much cancellation as the ideal case – however an increase in the number of taps will increase the cancellation. To apply multipath, a simple 15 tap FIR filter was convolved with the received data signal. Theoretically, this will mean that the channel memory only lasts for 15 taps and the cancellation should saturate beyond 15 taps. The higher bandwidths are clearly more affected by the channel and therefore aren't cancelled as well. Using more taps, however,

will yield better cancellation results for both the lower and higher bandwidths as can be seen again in Figure 3.9. The desired RX signal is still buried inside this signal and thus will not be seen by the demodulator. We can also observe cancellation vs symbol rate in Figure 3.10. Higher data rates suffer from multipath more due to the fact that the coherence bandwidth is small in a multipath environment.

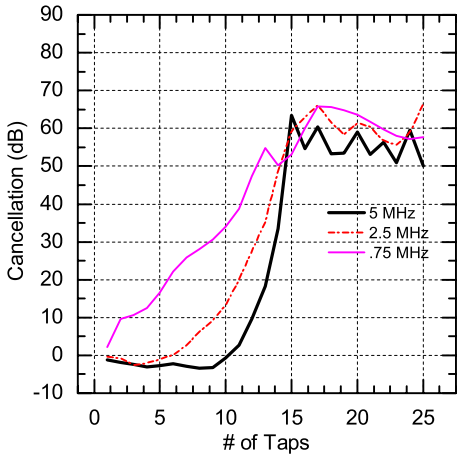

Figure 3.9 - Cancellation vs. taps for a QPSK signal over three different bandwidths

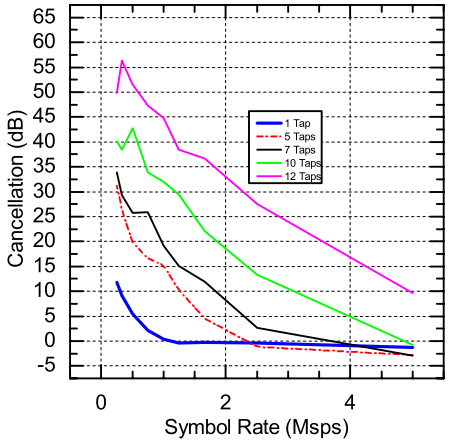

Figure 3.10 - Cancellation vs symbol rate for a QPSK signal with the number of taps set to 1, 5, 7, 10, and 12

To prove that the system can properly demodulate signals, we will now show SER vs. SNR curves for half duplex operation. Typically, the x-axis variable is Eb/No however, we can use SNR to prove that the demodulator works. The curves for an 8PSK modulation scheme are shown in Figure 3.11. It should be noted that a very large amount of data is needed to make the curves more accurate (billions of transmitted bits). Due to time constraints and processing capabilities of the computer used, only a small amount of data can be processed which explains the disjointed curves. Moreover, higher bandwidths will inherently have higher noise powers due to the 10*log(B) term.

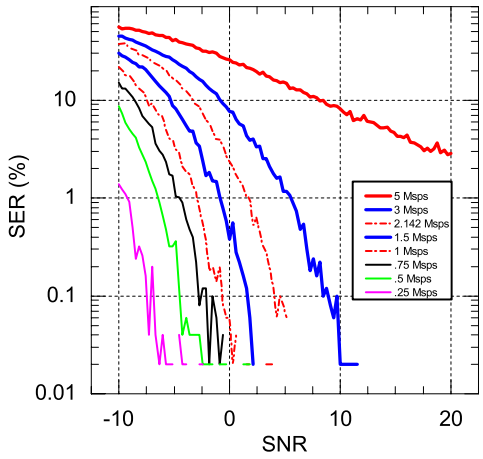

Figure 3.11 – Half Duplex SER vs SNR curves for an 8PSK modulation scheme

If we plot the symbol error rate (SER) vs the relative signal power of the received signal, we will get the results shown in Figure 3.12. Note that multiple 8PSK bit rates are shown below and it is clearly evident that cancellation is worse at higher bandwidths. It must be stated that this should not be construed as a BER vs Eb/No curve; however, they are analogous in the sense that the transmitted signal is indeed acting as noise. If we view

each signal with cancellation on and off, we can clearly see the improved symbol error rates. This is shown in Figure 3.13.

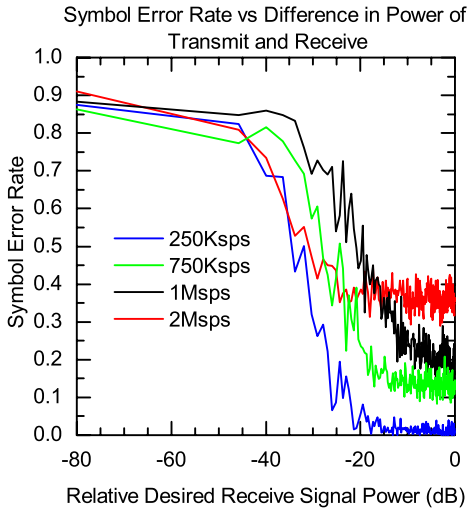

Figure 3.12 - Degradation of SER with decreasing signal power

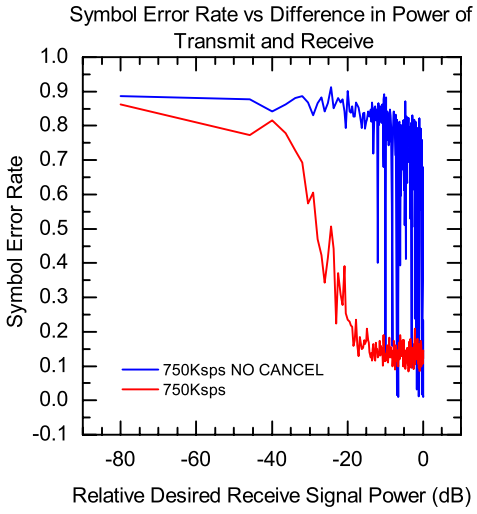

Figure 3.13 - Comparison of SER with cancellation turned on or off for a 750Ksps 8PSK modulated signal

From the simulations, it is clear that the cancellation increases with the number of taps and decreases with the symbol rate. The symbol rate error also decreases with the cancellation turned on and thus, we are sure that the system is working.

As a further observation, we will now show how the frequency response of the LMS FIR filter is affected by the bandwidth used. These effects are seen in Figure 3.14.

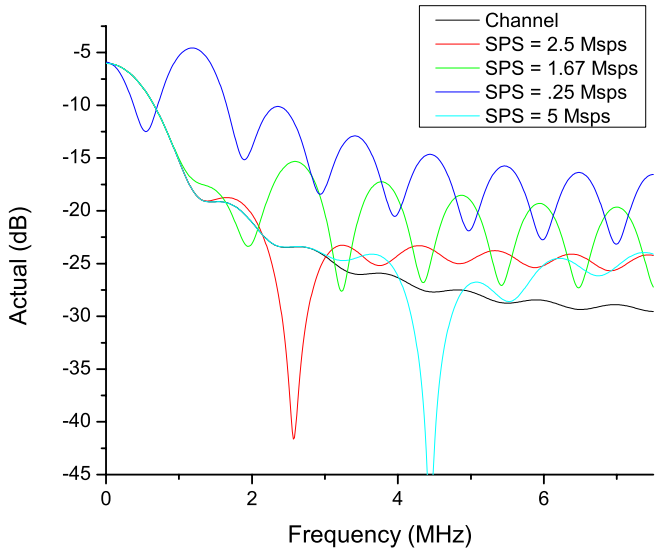

Figure 3.14 - Effect of symbol rate on the LMS coefficients

The coefficients are determined mainly by in-band coefficients and therefore, the subsequent predicted channel will match the actual channel model only for the relevant bandwidth. This may have an adverse effect on out of band interference signals and noise which will exert additional strain on the digital channel filter in practical transceivers.

CHAPTER 4

EXPERIMENT RESULTS

Section 4.1. – Characterization of the TX and RX chain

The system board (shown in Figure 4.1) was design using a Rogers 04003 dialectric. Coplanar-waveguide-with-ground type traces were used for matching RF lines to 50 Ohms. The 4-layer board was designed using Cadence Orcad.

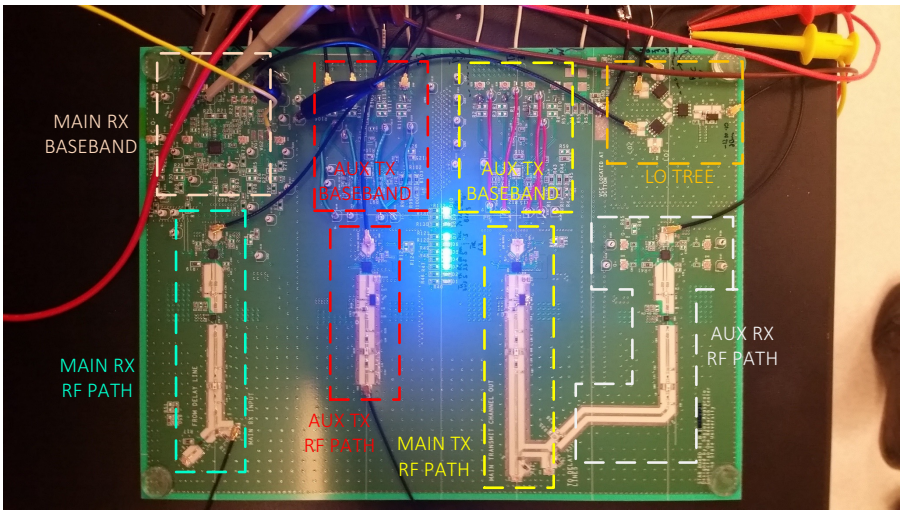

Figure 4.1 - System board

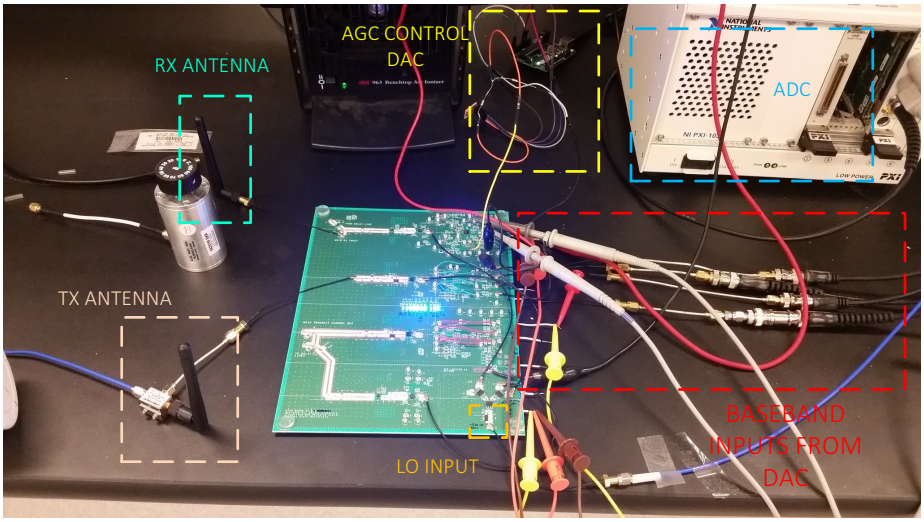

Figure 4.2 - System board integrated with bench top equipment. The transmit and receive antennas can be seen on the left.

The system setup is shown in Figure 4.2. After all DC voltages were set and confirmed, a small signal sine wave was applied to the input to observe the output RF. After this test, modulated data from the DAC was sent into the system to observe the output. After nominal operation of the TX channel was confirmed, the RX channel was tested.

With the board operational, a sine wave power sweep test was performed to observe the output non-linearity. The maximum output saturation power is 14.8 dBm which yields an OIP3 of roughly 25 dBm. To test for this, the Q channel was turned off and a simple sine wave was fed into the I channel. This results in a DSB-SC type signal at RF which is ideal for testing third-order non-linearity. The two tones will mix due to the non-linearity and produce tones at $2\omega_2 - \omega_1$ and $2\omega_1 - \omega_2$. These non-linear tones can clearly be seen in the Figure 4.3. The calculated OIP3 values over the output power and frequency extremes are shown in Table 4.1.

Table 4.1 - Calculated OIP3 values

Frequency (MHz)	IM3 (dB)	H1 (dBm)	OIP3 (dBm)
0.25	45.00	4.00	26.50
0.25	30.00	8.50	23.50
5.00	44.00	4.00	26.00
5.00	30.00	8.53	23.53

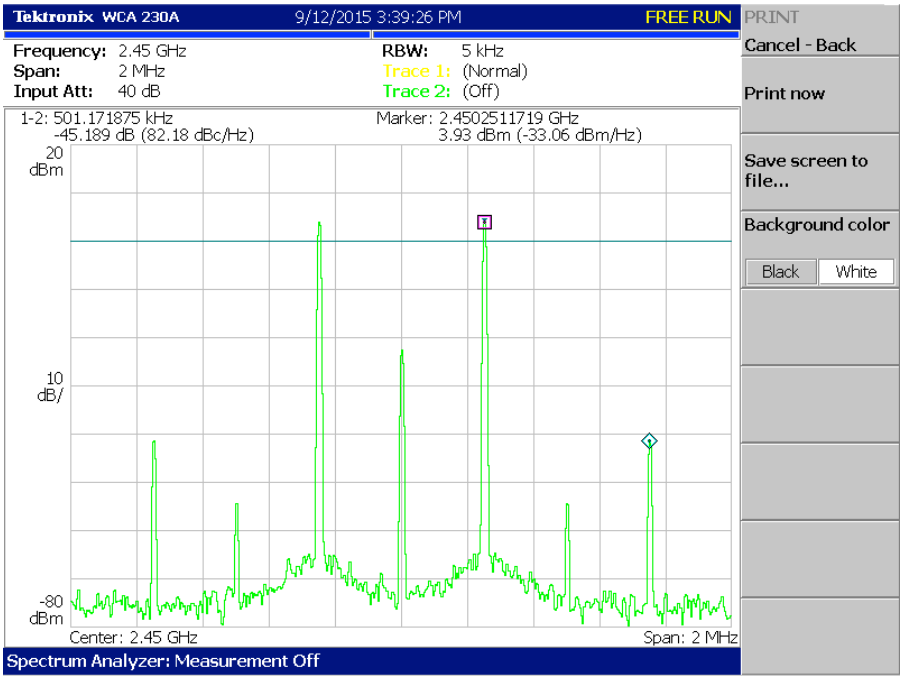

Figure 4.3 - Example output spectrum of a DSB-SC signal. The non-linear tones can clearly be seen.

These values correspond to the theoretical estimated OIP3 value of 25 dBm.

The RF TX output spectrum is shown in Figure 4.4. for an 8PSK modulated data signal with a 250 k symbol rate. The two peaks correspond to the DSB signal created by the modulator. The center tone is LO feedthrough and the smaller side tones are products of non-linearity. The channel bandwidth is chosen to be about (1+ β)/(2T) where β is the roll off factor of the root raised cosine filter and T is the symbol period. In this case, the DSB bandwidth is about 312 kHz (rounded down to 300 kHz in the spectrum analyzer). The effects of non-linearity are clearly present in the form of ACPR. The adjacent power rejection was found to be about 18 dB.

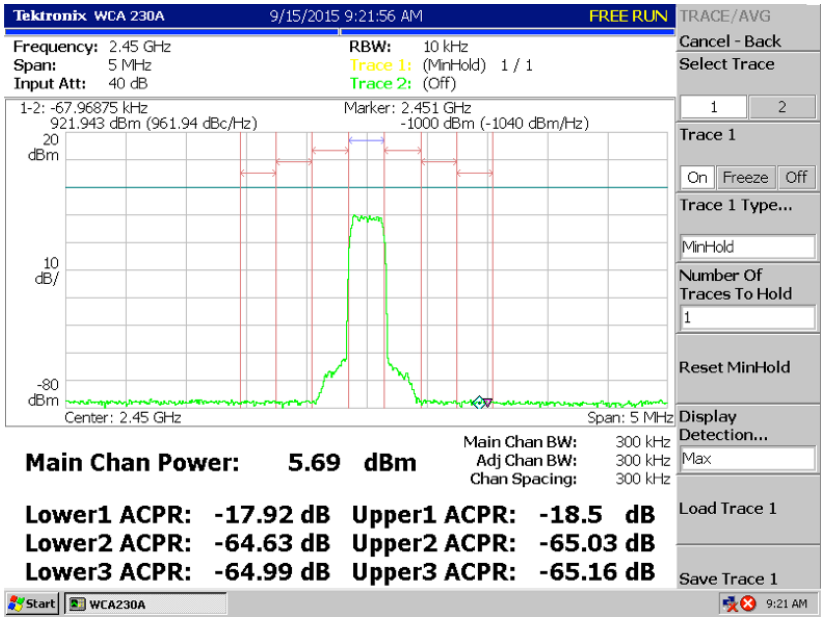

Figure 4.4 - TX RF output spectrum for an 8PSK modulated 250 Ksps data signal.

Finally, a sweep of output power vs. input voltage was performed to characterize the gain of the system. The results are shown in Figure 4.5.

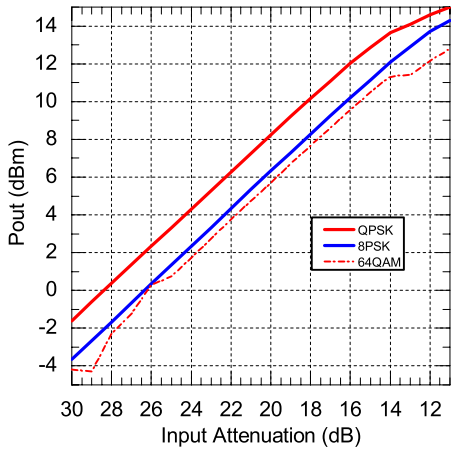

Figure 4.5- Output channel (or single tone) power vs. input voltage attenuation.

With the TX portion of the board fully tested and verified, the RX portion of the board was checked with the LMS algorithm. A coherent LO is used for both the TX and RX and therefore we don't have to worry about carrier recovery or even carrier phase noise.

Section 4.2. – Characterization of adaptive baseband interference cancellation

As stated earlier, the received constellation will be rotated by a certain angle dependent on the delay between the TX modulator and the RX demodulator path. Evidence of this is shown in Figure 4.6.

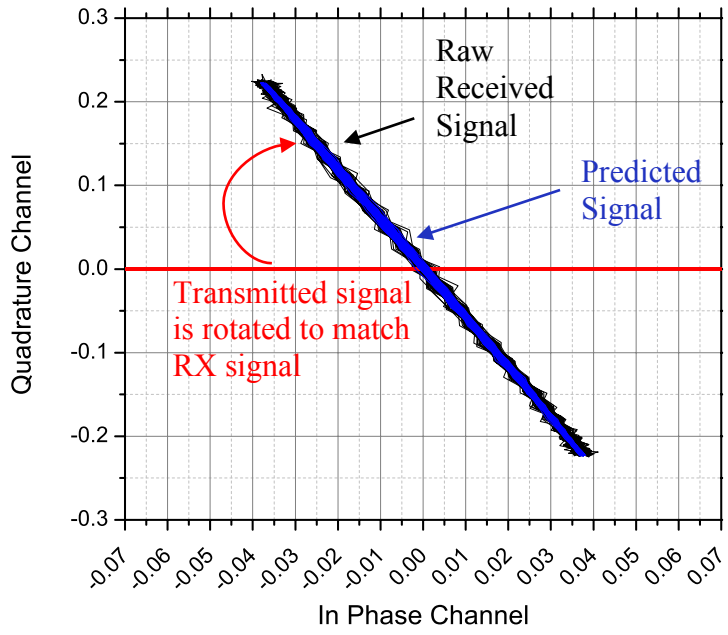

Figure 4.6 - Received and fixed constellation for the sine wave.

We can also observe the effects of the channel on a 5 Msps data stream. Shown in Figure 4.7, we observe the transmitted spectrum (with only quantization noise) and the received spectrum (with component and channel noise).

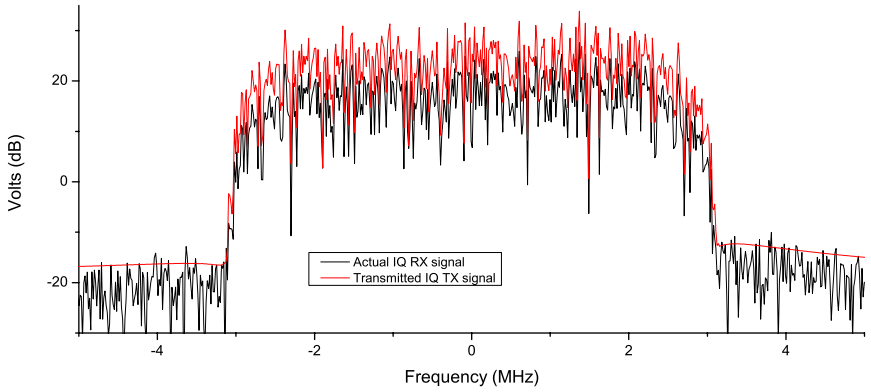

Figure 4.7 – Comparison of the transmitted spectrum with the received spectrum

If we plot the channel transfer function $H(f) = \frac{|IQ_{RX}(f)|}{|IQ_{TX(f)}|}$ we will observe the curves shown in Figure 4.8. Three different antenna positions were chosen to show how the environment is affected. The third position had multiple objects placed near the antennas to introduce more multipath and thus has a more varied shape.

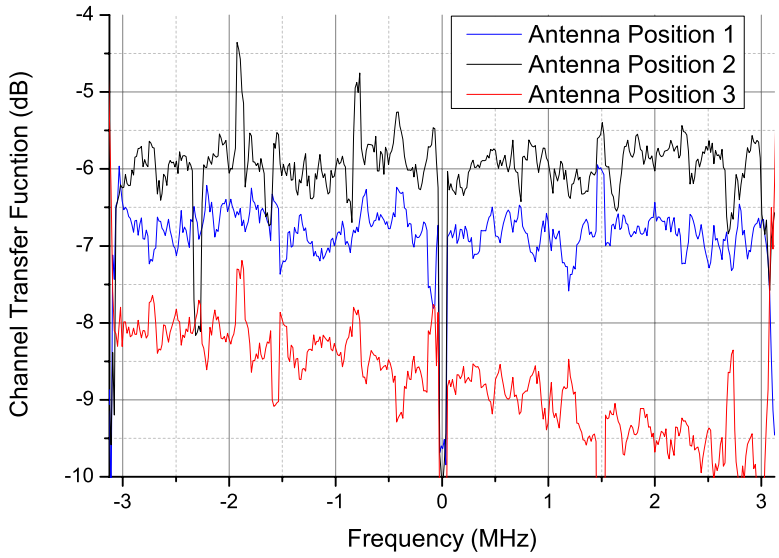

Figure 4.8 – Channel transfer functions

To test the LMS algorithm, the following sequences were performed. The data was first created in MATLAB and downloaded onto the DAC. Since the data is random and white, the same sequence can be used repeatedly without loss of generality. The DAC was set to repeatedly transmit the data in a circular fashion. Initially, burst mode transmission was desired, however, the machine was faulty and introduced settling time into the transmission which rendered the data unusable. A coarse correlation is then performed on the magnitudes of the RX and TX signals to correct for the delay introduced by the system and the circular transmission. Automatic phase control is inherently performed by the LMS algorithm since the coefficients are complex. The LMS algorithm then crawls through the data packet and compares/correlates each TX and RX sample with each other (in addition to the summed FIR taps). After the algorithm has finished running through the first packet, a second RX packet is sampled. The last coefficient values are used as seeds for the second packet and the process is repeated for a finite duration of time.

To show that the LMS algorithm is working, snap shots of the first several packets were taken. A sine wave was transmitted at 3.75 MHz in baseband at an output power of 6.08 dBm. Figure 4.9 shows the first packet of data received after being processed by the LMS algorithm with a 12 tap FIR filter. The scale factor μ was set to 0.3.

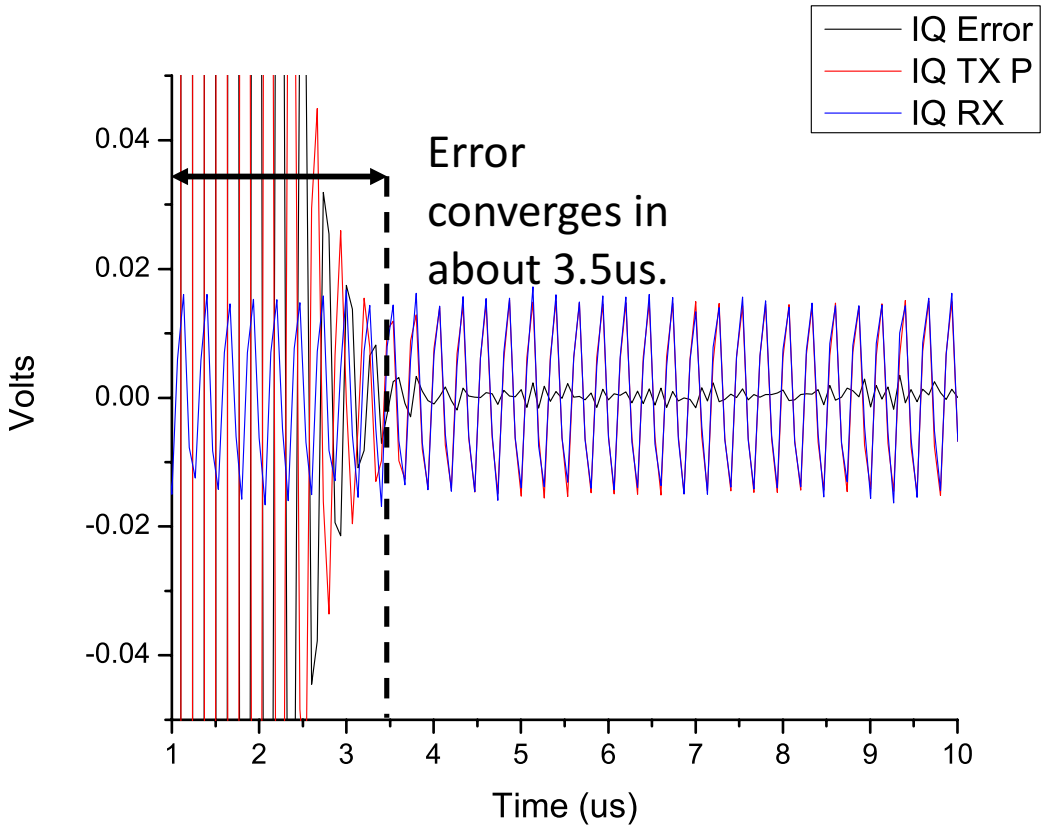

Figure 4.9 - First sine wave packet of data received.

It is evident that the error signal has converged to nearly zero volts and that the signal is being cancelled. It must be noted that convergence time for a sine wave is much quicker than for data. If we view the spectrum for similar signals in Figure 4.10, it becomes more apparent that the main interference tone has been cancelled by roughly 70 dB.

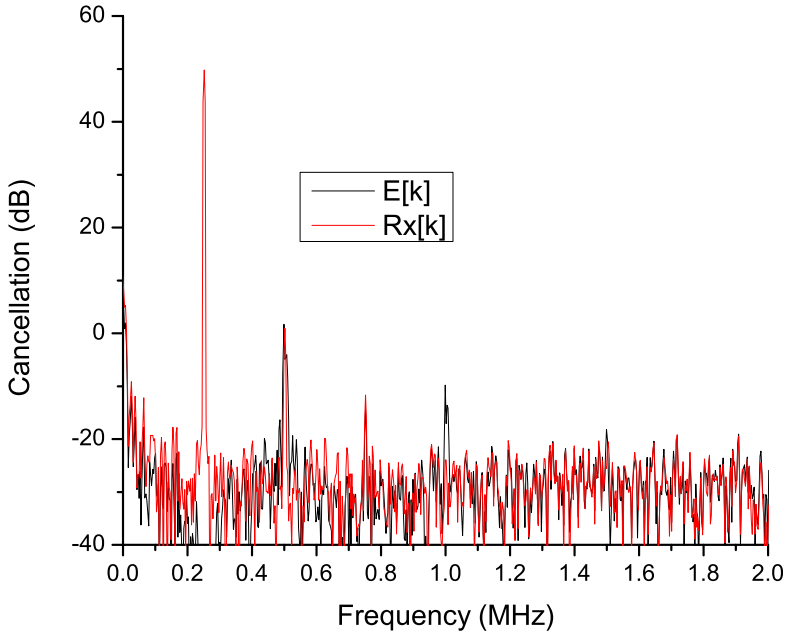

Figure 4.10 - Effect of cancellation in the frequency domain on a sine wave at 250 KHz.

The magnitude of the LMS filter coefficients over packets is shown in Figure 4.11 to indicate convergence.

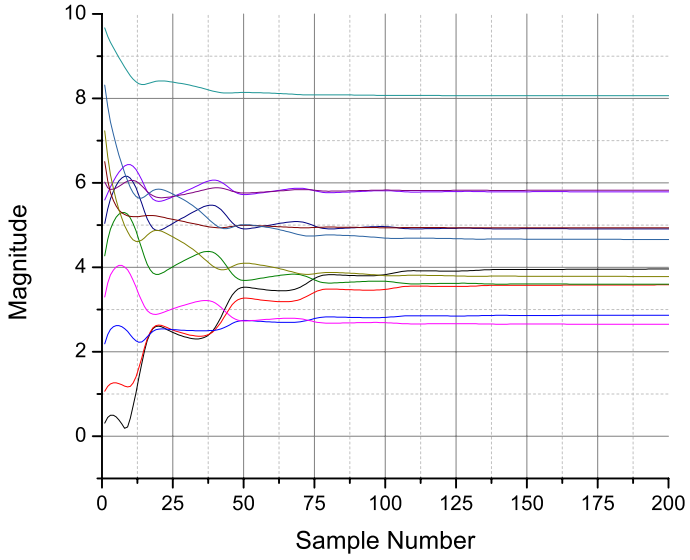

Figure 4.11 - Coefficient magnitudes converging.

If we change the μ factor in the LMS algorithm, the convergence time should decrease. An experiment was performed to observe the effect of the μ factor on convergence time for an 8PSK signal at 1Msps with 12 FIR taps. Note that the convergence times will change depending on the data scheme and number of taps – the aforementioned parameters are used solely as an example to observe change in convergence time. The results are shown in Figure 4.12. Note that all times are below the 100 ms of required re-calibration time stated in [1].

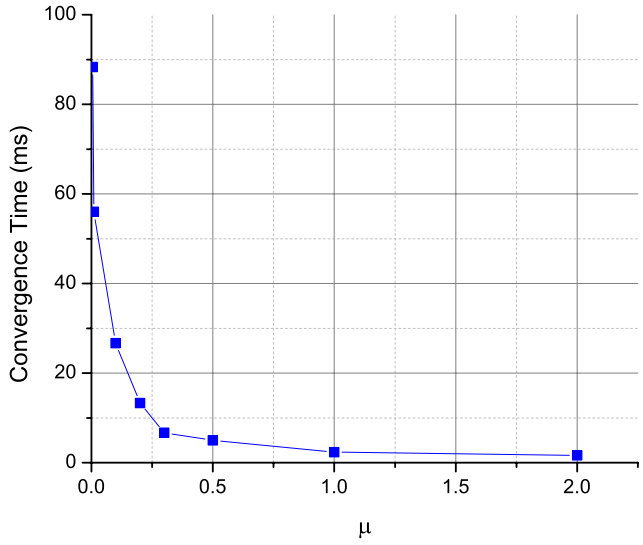

Figure 4.12 – The effect of μ on convergence time

Having proven that the LMS system was working, a variety of sweeps was performed to determine what parameters affect cancellation. Figure 4.13 represents the test setup.

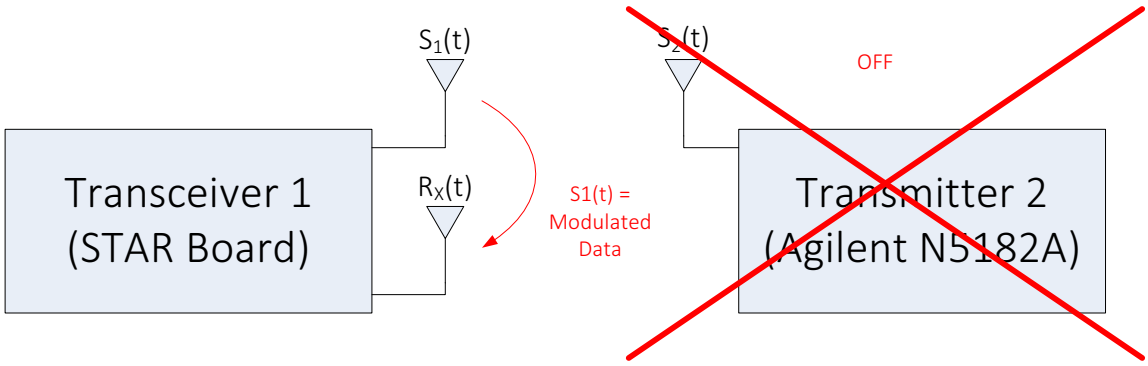

Figure 4.13 - First full duplex test case

We first observe how cancellation is affected by the symbol rate. According to the simulations, we should see a fall in cancellation as the bandwidth increases. The number of taps was held at 1 and the output power was recorded for a QPSK modulation scheme. The results are shown in Figure 4.14. Note that the AGC was online for all these experiments.

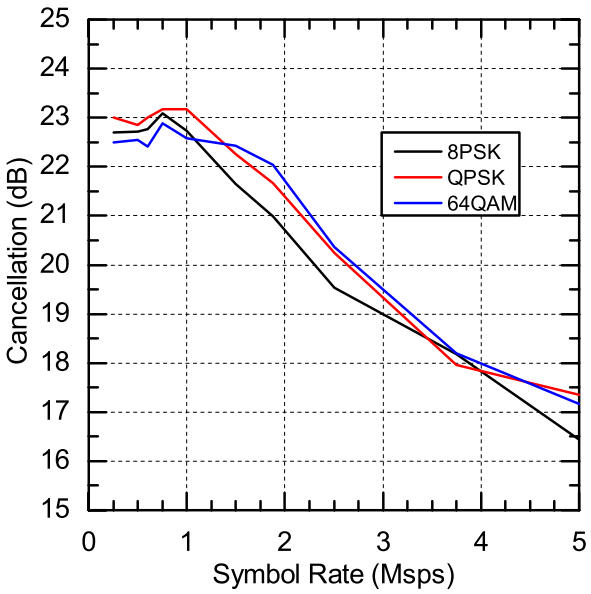

Figure 4.14 - The effect of symbol rate on cancellation for a QPSK/8PSK/64QAM signal with 1 tap.

From this graph, we can see a clear downwards trend in cancellation as the bandwidth of the signal increases. The bandwidth and number of taps were held constant and the cancellation was recorded over the RF TX output power. As the output power of the TX channel increases, the harmonic distortion and non-linearity also increase and thus the system will not be able to perform cancellation as well. The results are shown on Figure 4.15 and 4.16 for both a causal and non-causal FIR filter using QPSK and 8PSK modulation schemes. As discussed in [1], implementing a non-causal filter in the system allows the LMS algorithm to more accurately model the received wave – using transmitted samples on both sides (time-wise) of the received sample is analogous to sinc interpolation. In all the cases, we can clearly see that as the output power increases, the cancellation increases until the system enters saturation in which the harmonic distortion becomes quite high.

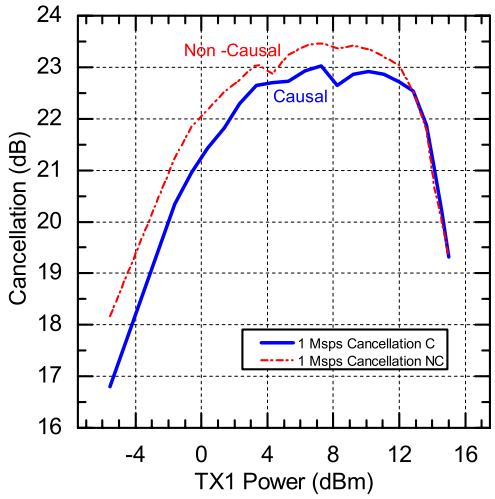

Figure 4.15 - Effect of TX output power on cancellation for a QPSK signal.

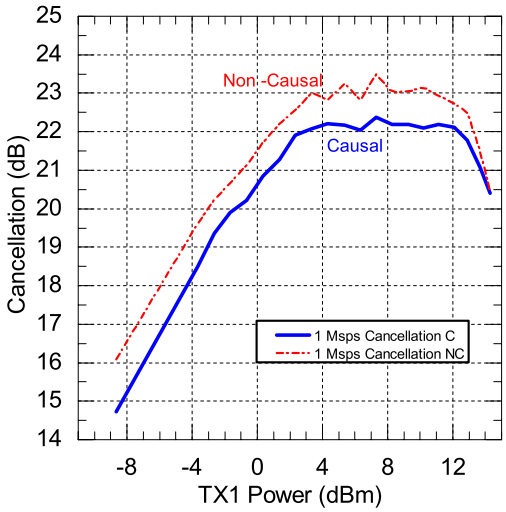

Figure 4.16 - Effect of TX output power on cancellation for an 8PSK signal

For weak transmit powers, the AGC struggles to maintain the full scale range (FSR) of the ADC and thus the cancellation is not as high as it can be. Once the FSR is obtained, the cancellation remains constant until the non-linearity becomes significant in which case the cancellation drops off.

Next, we show how the cancellation is affected based on the number of taps used in the LMS FIR filter. Theoretically (as was seen in the simulations) an increase in the number of taps should increase the cancellation. The measured results for three modulation schemes are shown below in Figure 4.17.

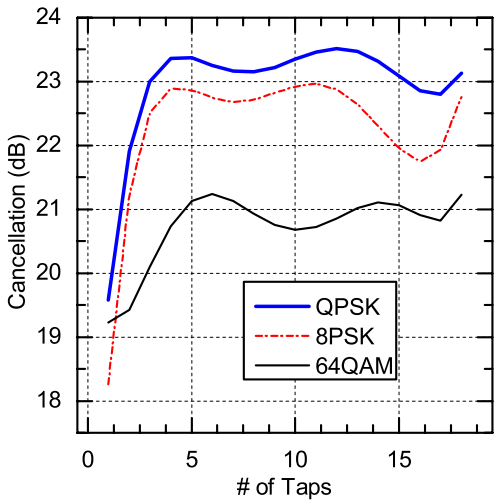

Figure 4.17 - Effect of FIR taps on cancellation for a QPSK signal

It is evident that an increase in taps will affect the cancellation positively. However, owing to the large delay between taps due to the sampling rate, the channel memory is only predicted by the first few taps and thus only a finite amount of cancellation is obtained. Increasing the taps beyond roughly 5-6 taps will not increase the cancellation significantly anymore.

Section 4.3. – Characterization of full duplex operation

Finally, we show how the symbol error rate (SER) performs with cancellation over the transmitter output power. The output power of the transceiver (TX1) was swept while the actual data from a secondary transmitter (TX2) was transmitted at a maximum power of 10 dBm using a directional antenna at a distance of about 25 cm away from the RX antenna. A simple diagram of this is shown in Figure 4.18. The data used for each transmitter was completely uncorrelated. We will first show how the system performs in a half-duplex environment. This test will act as a control and prove that the system is working

nominally. Figure 4.19 contains the SER curves for half duplex operation. It must be noted that SER is used as opposed to the BER since the SER is a more analog metric. The BER is can be affected by forward error correction (FEC) or grey coding which are digital mechanisms.

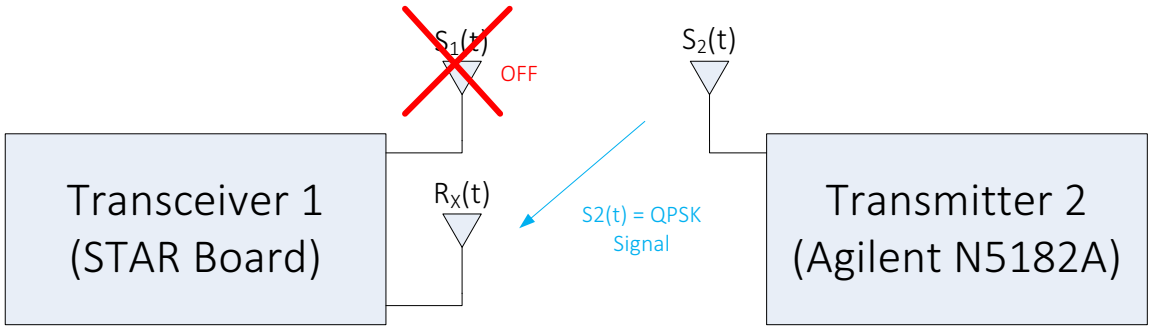

Figure 4.18 - First setup for half duplex testing

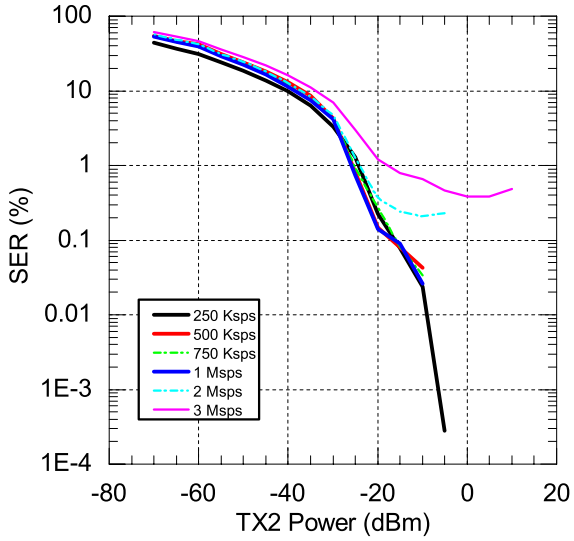

Figure 4.19 - Symbol Error Rate vs TX2 Output Power for Half Duplex Operation

For 2 and 3 Msps, the oversampling ratio (OSR) and bandwidth affect the demodulation adversely as shown in the simulations. Moreover, due to synchronization issues between the ADC and DAC, the demodulation will be adversely affected at higher bandwidths. To further test the system, a song was successfully transmitted over the air with zero bit errors at high transmit power. Grey coding was used for this particular test.

After the half duplex control test, the full duplex tests were performed. The first test case is shown in Figure 4.20.

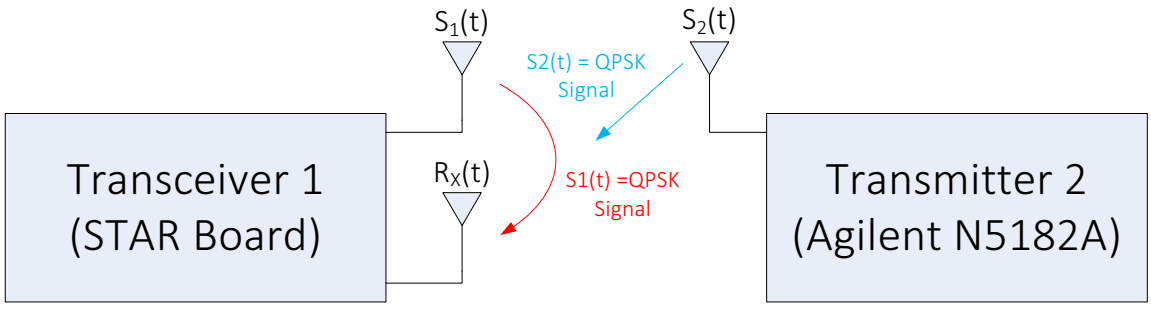

Figure 4.20 - Final full duplex test case with desired data

The same SER test was performed with cancellation turned on for a QPSK signal with various symbol rates. The TX1 power was set to 10.15 dBm and the antenna placement was about 25 cm away which equates to roughly 28 dB of loss, resulting in a receive power of -18 dBm. The TX2 power was then varied – the results are shown in Figure 4.21. The number of taps used is 12 with a causal FIR filter.

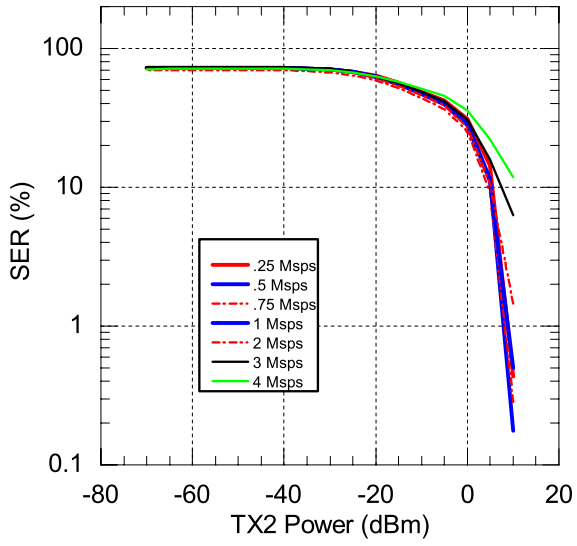

Figure 4.21 - SER curves for full duplex operation

While it appears that the system is working, the results will not be feasible for any practical application due to the fact that only digital cancellation is used. The cancellation needed is nearly 100 dB and only 20-23 dB of cancellation in the digital realm was achieved with an additional 28 dB in the RF domain due to antenna separation. However, we have successfully shown that the LMS algorithm works as an online adaptive filter which requires no prior knowledge of the channel thus eliminating the need for pilot tones or preambles. We can compare full duplex with half duplex operation to observe the difference in performance in Figure 4.22.

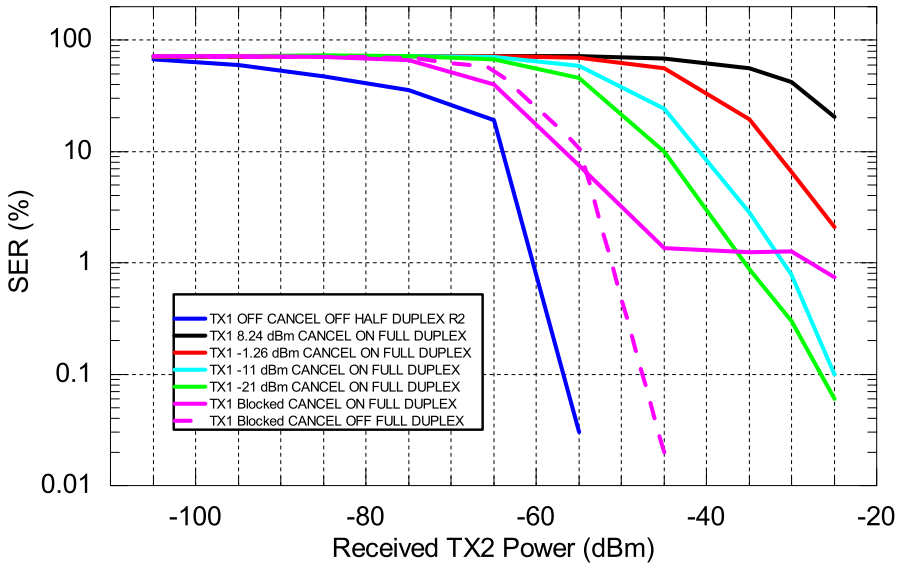

Figure 4.22 - Comparison of half duplex and full duplex operation

It is once again clear that the half duplex operation performs better. However, if the received interference signal is reduced (effectively increasing the analog RF cancellation) the SER of the system improves. If we look at Figure 4.23, we observe that turning off the cancellation yields worse results which is evidence that the LMS cancellation algorithm is working correctly.

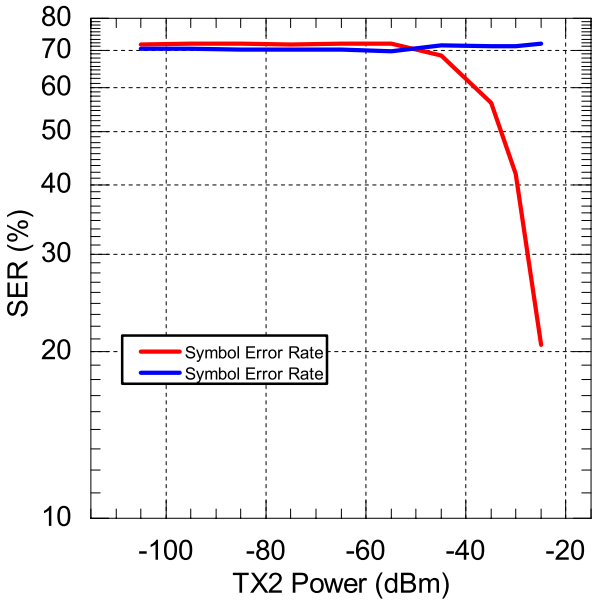

Figure 4.23 - Effects of turning the cancellation on or off

It must be noted that at this high TX2 power, the ADC is mainly dominated by the TX2 strength and therefore the cancellation is not as high as it could be in the digital domain which implies that additional RF cancellation is needed [6]. This statement is further corroborated by the cancellation vs. power graphs shown earlier.

CHAPTER 5

CONCLUSION AND DISCUSSION

Section 5.1. – Analysis of Experimental Data

From the data gathered, it is clear that the LMS algorithm can provide a real time online solution for echo cancellation. The results showed us that bandwidth, TX output power, the number of taps, and the received strength of the desired data affect cancellation. There were numerous issues with this experiment, namely:

1. The ADC and DAC were not synchronized. Even though only short bursts of data were transmitted, jitter and other periodic effects due to the unsynchronized clocks that might have occurred during this burst will have affect the cancellation result.
2. The LMS algorithm was only implemented in the digital domain. The TX1 signal completely saturated the ADC at high powers and thus this system will not be of practical use without RF and analog baseband cancellation techniques. This experiment was meant as a proof of concept.
3. The TX VGAs were fried early in the experiment. After changing input capacitors for the TX chain, the VGAs stopped working. The input impedance was measured as nearly 8 Ohms which was completely off from the specified 400 Ohms. Thus, the VGAs had to be removed completely and the output power was then managed by the output attenuation of the DAC itself. This limited the full scale range of the DAC and thus quantization noise was increased.
4. MATLAB could only process data sequentially. This is the reason why this experiment can be considered pseudo-real time and not actual real time.

5. The burst capability of the TX2 data was broken inside the machine. This meant that the time synchronization of data bursts could not be implemented. A workaround for this issue was to leave the TX2 in continuous reset mode which meant that the data kept repeating over and over. This data was then circularly shifted inside MATLAB after a cross correlation function was completed. This meant that a discontinuous jump existed somewhere inside the data packet – this may have contributed to some symbol errors.

Section 5.2. – Future improvements

The biggest improvement for the full duplex system is implementing the LMS algorithm at RF. This will cancel out both TX phase noise and distortion. The multipath issue can be resolved by using multiple delay paths before injection the signal to emulate an FIR type adaptive filter. Moreover, this will ensure that the TX1 data will not saturate the ADC and thus provide a better SNR overall.

The use of an FPGA with an integrated DAC/ADC will also greatly improve the robustness and quality of the experiment. The converters will be both controlled by the same clock and the processing will be parallel.

REFERENCES

[1] D. Bharadia, E. McMilin, and S. Katti, "Full duplex radios," *SIGCOMM '13 Proc. ACM SIGCOMM 2013 Conf. SIGCOMM*, vol. 43, no. 4, pp. 375–386, 2013.

[2] J. Il Choi, M. Jain, K. Srinivasan, P. Levis, and S. Katti, "Achieving Single Channel, Full Duplex Wireless Communication."

[3] M. Duarte and A. Sabharwal, "Full-Duplex Wireless Communications Using Off-The-Shelf Radios : Feasibility and First Results," pp. 1558–1562, 2010.

[4] E. Everett, M. Duarte, C. Dick, and A. Sabharwal, "Empowering full-duplex wireless communication by exploiting directional diversity," *Conf. Rec. - Asilomar Conf. Signals, Syst. Comput.*, pp. 2002–2006, 2011.

[5] M. Jain, J. Il Choi, T. Kim, D. Bharadia, S. Seth, K. Srinivasan, P. Levis, S. Katti, and P. Sinha, "Practical, real-time, full duplex wireless," *Proc. 17th Annual. Int. Conf. Mob. Comput. Netw. (MobiCom '11)*, p. 301, 2011.

[6] A. Sahai, G. Patel, C. Dick, and A. Sabharwal, "On the impact of phase noise on active cancelation in wireless full-duplex," *IEEE Trans. Veh. Technol.*, vol. 62, no. 9, pp. 4494–4510, 2013.

[7] W. Di, Z. Can, G. Shaoshuai, and D. Chen, "A Digital Self-Interference Cancellation Method for Practical Full-Duplex Radio," 2014.

[8] A. Siddig, C. J. Bleakley, A. Makki, M. M. Saad, and J. R. Cavallaro, "High-resolution time of arrival estimation for OFDM-based transceivers," *Electron. Lett.*, vol. 51, no. 3, pp. 294–296, 2015.

[9] K. McClaning, *Wireless Receiver Design for Digital Communications*. Raleigh, NC: SciTech Publishing, 2012[10] Y. S. Choi and H. Shirani-Mehr, "Simultaneous transmission and reception: Algorithm, design and system level performance," *IEEE Trans. Wireless. Communications.*, vol. 12, no. 12, pp. 5992–6010, 2013.

[11] M. Duarte, A. Sabharwal, V. Aggarwal, R. Jana, K. K. Ramakrishnan, C. W. Rice, and N. K. Shankaranarayanan, "Design and characterization of a full-duplex multiantenna system for wifi networks," *IEEE Trans. Veh. Technol.*, vol. 63, no. 3, pp. 1160–1177, 2014.

[12] E. Everett, A. Sahai, and A. Sabharwal, "Passive Self-Interference Suppression for Full-Duplex Infrastructure Nodes," vol. 13, no. 2, pp. 680–694, 2014.

[13] M. a. Khojastepour, K. Sundaresan, S. Rangarajan, X. Zhang, and S. Barghi, "The case for antenna cancellation for scalable full-duplex wireless communications," *Proc. 10th ACM Work. Hot Top. Networks - HotNets '11*, pp. 1–6, 2011.

[14] B. Radunovic, D. Gunawardena, P. Key, A. Proutiere, N. Singh, V. Balan, and G. Dejean, "Rethinking Indoor Wireless: Low Power, Low Frequency, Full-duplex," *Microsoft Tech. Rep.*, p. 7, 2009.

[15] D. Duet, "AN ASSESSMENT OF DUPLEXING METHODS FOR THE RADIO LINKS," pp. 1–5, 1992.

[16] S.C. Douglas, *Introduction to Adaptive Filters.* Boca Raton, FL: CRC Press LLC, 1999

[17] J.A. Apolinario, *QRD-RLS Adaptive Filtering*. Springer Science+Business Media, LLC, 2009

APPENDIX A

MATLAB CODE

```
for k = N*crawl_delay:crawl_length


        % Assign the FIR delays.
        for j = 0:N-1
            % Comment one section or the other to use interpolation.
            %IQ_TX_delay(N-j) = IQ_transmit_xcd(k-j);
            %IQ_TX_x(N-j) = IQ_transmit_xcd(k-j)*conj(w(j+1));
            IQ_TX_delay(N-j) = IQ_transmit_xc_int(k+delay_offset-
            (j*crawl_delay));
            IQ_TX_x(N-j) = IQ_transmit_xc_int(k+delay_offset-
            (j*crawl_delay))*(conj(w(j+1)));
        end

        % Sum the signals. Since we are starting at N,
        % this is the Nth value.
        IQ_TX_sum = sum(IQ_TX_x);

      % Here, the error is computed by subtracting the received from    %
transmitted filtered sum. It is assumed that the delay is within
        % N samples of the transmitted signal otherwise there won't be
        % enough delay to compensate and N will have to be increased.

        % Comment one section or the other to use interpolation
        %error_sum = IQ(k) - IQ_TX_sum;
        error_sum = IQ_receive_int(k) - IQ_TX_sum;
        error_wave(k) = error_sum;
        IQ_wave_test(k) = IQ_TX_sum;
        output_cor = conj(error_sum) * fliplr(IQ_TX_delay);
        w = w + ((.3)*output_cor);
%         display(sprintf('w1 is %d',w(1)));
%         display(sprintf('w2 is %d',w(2)));
%         display(sprintf('w3 is %d',w(3)));
%         display(sprintf('w4 is %d',w(4)));
%         display(sprintf('w5 is %d',w(5)));
%         display(sprintf('output_cor is %d',output_cor));
%         display(sprintf('error sum is %d',error_sum));
%         display(sprintf('IQ_TX_delay is %d',IQ_TX_delay));
        %pause
    end
```